Robust Internal-Force Based Impedance Control for Coordinating Manipulators - Theory and Experiments

Robert G. Bonitz and T.C. Hsia

Abstract

A robust internal force-based impedance control scheme for coordinating manipulators is introduced. Internal force-based impedance control enforces a relationship between the velocity of each manipulator and the internal force on the manipulated objects and requires no knowledge of the object dynamic model. Each manipulator's nonlinear dynamics is compensated by a robust auxiliary controller which is insensitive to robot-model uncertainty. The controller is only weakly-dependent on each manipulator's inertia matrix. The scheme is computationally inexpensive and suitable for general-purpose microcomputer implementation. Stability of the system is analyzed including the effects of computational delays on both a single-arm manipulator in contact with a rigid surface and a dual-arm system manipulating a rigid object. We show that the inertia matrix has a lower bound with respect to the estimated manipulator Cartesian end-point inertia which is independent of the sampling period. Rigorous experimental investigations are performed and the results presented which validate the proposed concepts.

Keywords

Internal force, impedance control, coordinating, manipulator, robot, delay.

I. Introduction

Multiple robots performing tasks together in a coordinated manner can have a significant advantage over a single robot when executing tasks such as material transport of heavy items, assembly of manufactured items, space-based manipulation, etc. Controllers for coordinating multiple robots proposed during recent years may be generally classified as position/force control [1], [2], [3] or impedance control [4], [5], [6], [7], [8]. In position/force control the extra degrees of freedom of the multiple arm system are used to control internal force. The required joint torques are the sum of torques from the position and force control loops. Impedance control has generally been implemented by adding an admittance/compliance loop around the position controller to regulate the contact force. It has been shown that the gain of the admittance function must be limited to assure stability [9].

In [10] the theory of an internal force-based impedance control scheme was proposed which enforces a relationship between the velocity of each manipulator and the internal force on the manipulated objects. It has the advantage that kinematic relationships are used to compute the internal force and no knowledge of the object's dynamics is required. Furthermore, because the impedance function is directly implemented, the gain restriction cited previously does not

R. Bonitz is currently with the Jet Propulsion Laboratory, Pasadena, CA.
T.C. Hsia is with the Systems, Control, and Robotics Laboratory, Dept. of Electrical and Computer Engineering, University of California, Davis, CA.
This work supported in part by the NITTA Corporation of Japan.

apply. The scheme does, however, require the dynamic model of each manipulator which may not be known exactly in practice.

The performance of [10] and other model-based schemes are critically dependent on knowledge of the manipulator dynamics. For a system of multiple coordinating manipulators handling a rigid object, model uncertainty is more significant than for a single manipulator operating in free space due the fact that position tracking errors can cause significant internal forces in the system. Actuator limits may be exceeded and damage to the manipulators or the object may occur. Thus, the practicality and performance of [10] and other similar schemes is critically dependent on the ability to deal with dynamic model uncertainty. In [11] robust Cartesian-based control schemes which require only minimal knowledge of the manipulator dynamic model were presented based on the robust joint-control schemes developed in [12], [13]. The nonlinear dynamics of each manipulator are compensated by a computationally simple robust auxiliary controller which has a time-invariant and time-delayed structure. In this paper the control schemes presented in [10] and [11] are integrated together to form a robust controller for multiple coordinating robots.

In practice the control laws will be implemented digitally. Computational delays can affect the stability of the system and will generally place bounds on the values of the controller parameters. Digital implementations of stiffness and damping control were examined for a single manipulator by Whitney in [14] which showed a tradeoff between bandwidth and the stiffness of the environment. In [15] Colgate showed that computational delays can exacerbate contact instability problems caused by noncolocation of sensors and actuators and that positive force feedback has a stabilizing effect. In [10] the effects of computational delays on internal-force based impedance control was analyzed and we showed that the controller inertia matrix has a lower bound with respect to the actual Cartesian endpoint inertia of the manipulator. In this paper we extend the analysis to a robust version of the controller presented in [10].

The purpose of this paper is to propose a solution to the robot model uncertainty problem, analyze the stability of the proposed controller including the effects of computational delays, and to perform a rigorous experimental study to test the practicality and performance of the proposed control scheme.

II. Robust Controller

A. Control Law Derivation

Consider the system of n robots handling a rigid object (or multiple objects in contact with each other) as shown in Figure 1. Each manipulator grasps the object rigidly and, thus, may exert both a force and a moment on the object. The dynamic equation for each manipulator is given by [10]:

$$\boldsymbol{\tau_i} = \boldsymbol{D_i}(\boldsymbol{q_i})\ddot{\boldsymbol{q}}_{\boldsymbol{i}} + \boldsymbol{E_i}(\boldsymbol{q_i}, \dot{\boldsymbol{q}}_{\boldsymbol{i}}) + \boldsymbol{J_i^T}(\boldsymbol{q_i})\tilde{\boldsymbol{f}}_{\boldsymbol{i}} \tag{1}$$

where $\boldsymbol{\tau_i}$ = joint torque vector of the *ith* robot

$\boldsymbol{D_i}$ = inertia matrix of the *ith* robot

$\boldsymbol{E_i}$ = Coriolis, centripetal, friction and gravity vector of the *ith* robot

$\boldsymbol{J_i}$ = Jacobian of the *ith* robot

$\boldsymbol{q_i}$ = joint position vector of the *ith* robot

$\tilde{\boldsymbol{f}}_{\boldsymbol{i}} = [\boldsymbol{f_i^T}\ \boldsymbol{m_i^T}]^{\boldsymbol{T}}$ = force and moment exerted by the *ith* robot end effector.

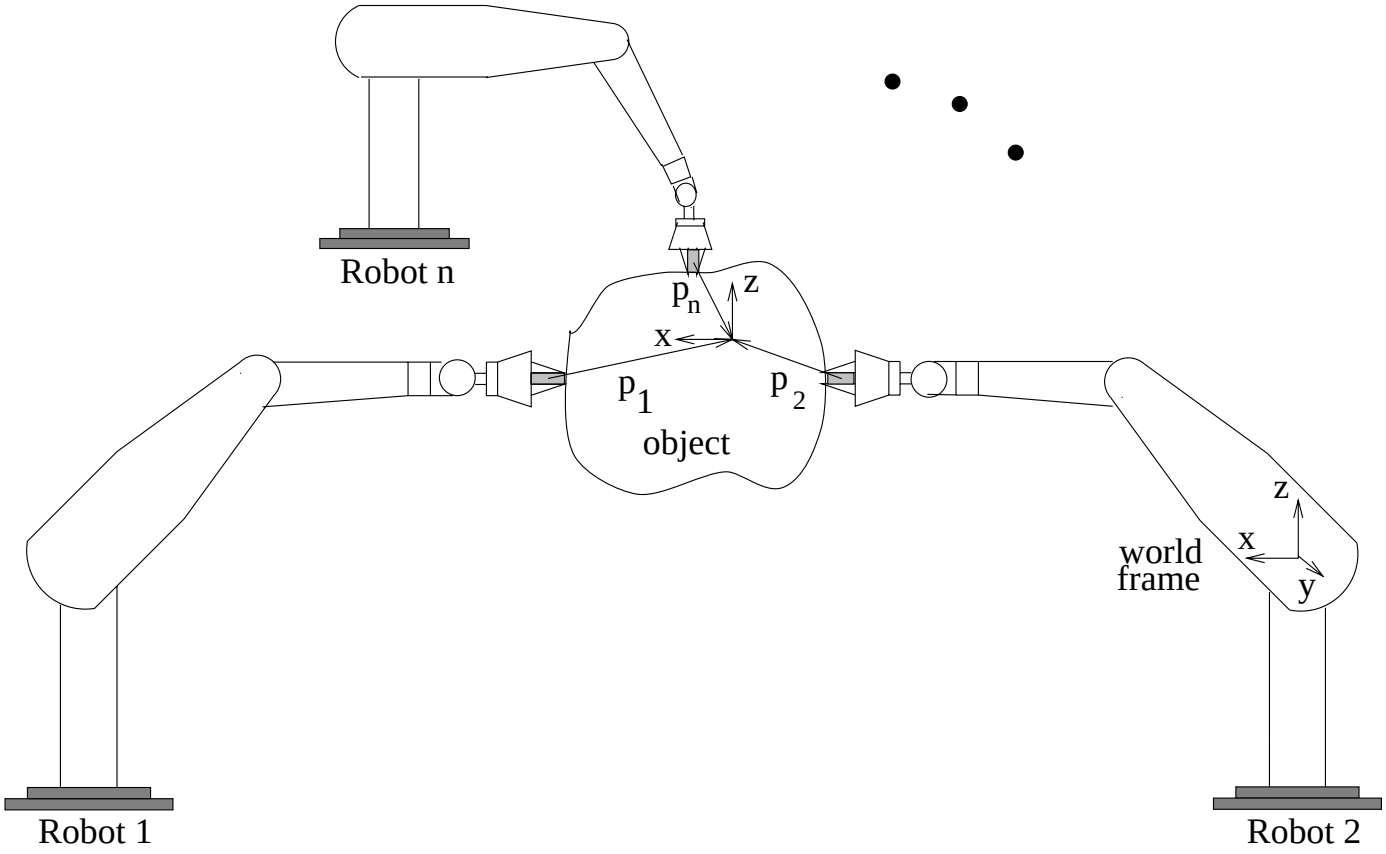

Fig. 1. n-Manipulator System

Let $\bar{\boldsymbol{D}}_{\boldsymbol{i}}$ be a constant diagonal matrix for each manipulator [13]. The determination of $\bar{\boldsymbol{D}}_{\boldsymbol{i}}$ will be discussed later. The preceding robot model is reformulated as

$$\boldsymbol{\tau_i} = \bar{\boldsymbol{D}}_{\boldsymbol{i}}\ddot{\boldsymbol{q}}_{\boldsymbol{i}} + \boldsymbol{H_i}(\boldsymbol{q_i}, \dot{\boldsymbol{q}}_{\boldsymbol{i}}, \ddot{\boldsymbol{q}}_{\boldsymbol{i}}) \tag{2}$$

where

$$\boldsymbol{H_i}(\boldsymbol{q_i}, \dot{\boldsymbol{q}}_{\boldsymbol{i}}, \ddot{\boldsymbol{q}}_{\boldsymbol{i}}) = \boldsymbol{E_i}(\boldsymbol{q_i}, \dot{\boldsymbol{q}}_{\boldsymbol{i}}) + \boldsymbol{J}_{\boldsymbol{i}}^{\boldsymbol{T}}(\boldsymbol{q_i})\tilde{\boldsymbol{f}}_{\boldsymbol{i}} + [\boldsymbol{D_i}(\boldsymbol{q_i}) - \bar{\boldsymbol{D}}_{\boldsymbol{i}}]\ddot{\boldsymbol{q}}_{\boldsymbol{i}}. \tag{3}$$

The first term on the right-hand side of (2) is linear. The second term, $\boldsymbol{H_i}$, contains all of the nonlinear dynamics of the manipulator including Coriolis, centrifugal, gravity, and friction forces along with the nonlinear configuration-dependent acceleration dynamics and externally applied forces.

If we choose the control input, $\boldsymbol{\tau_i}$, for the *ith* manipulator to be

$$\boldsymbol{\tau_i} = \bar{\boldsymbol{D}}_{\boldsymbol{i}}\boldsymbol{u_i} + \boldsymbol{H_i}(\boldsymbol{q_i}, \dot{\boldsymbol{q}}_{\boldsymbol{i}}, \ddot{\boldsymbol{q}}_{\boldsymbol{i}}), \tag{4}$$

then substituting (4) into (2) yields the double integrator system at each joint

$$\ddot{\boldsymbol{q}}_{\boldsymbol{i}} = \boldsymbol{u_i} \tag{5}$$

where $\boldsymbol{u_i}$ becomes the joint-level control input to be designed for the *ith* manipulator.

At this point, the computation of the control torque, $\boldsymbol{\tau_i}$, involves two terms - $\bar{\boldsymbol{D}}_{\boldsymbol{i}}\boldsymbol{u_i}$, which is simple to compute, and $\boldsymbol{H_i}(\boldsymbol{q_i}, \dot{\boldsymbol{q}}_{\boldsymbol{i}}, \ddot{\boldsymbol{q}}_{\boldsymbol{i}})$, which is quite complicated to compute and subject to uncertainty. The next step is to simplify the computation of $\boldsymbol{H_i}(\boldsymbol{q_i}, \dot{\boldsymbol{q}}_{\boldsymbol{i}}, \ddot{\boldsymbol{q}}_{\boldsymbol{i}})$. For convenience we drop the dependence of $\boldsymbol{H_i}(\boldsymbol{q_i}, \dot{\boldsymbol{q}}_{\boldsymbol{i}}, \ddot{\boldsymbol{q}}_{\boldsymbol{i}})$ on $\boldsymbol{q_i}$, $\dot{\boldsymbol{q}}_{\boldsymbol{i}}$ and $\ddot{\boldsymbol{q}}_{\boldsymbol{i}}$.

The control torque is modified to be

$$\boldsymbol{\tau_i} = \bar{\boldsymbol{D}}_{\boldsymbol{i}}\boldsymbol{u_i} + \widehat{\boldsymbol{H}}_{\boldsymbol{i}} \tag{6}$$

where $\widehat{\boldsymbol{H}}_{\boldsymbol{i}}$ is an estimate of $\boldsymbol{H_i}$. The problem is now reduced to developing a method of computing $\widehat{\boldsymbol{H}}_{\boldsymbol{i}}$.

First, we rearrange (2) which yields

$$\boldsymbol{H_i} = \tau_i - \bar{\boldsymbol{D}}_i\ddot{\boldsymbol{q}}_i. \tag{7}$$

If we assume that $\boldsymbol{H_i(t)}$, the value of $\boldsymbol{H_i}$ at time $\boldsymbol{t}$, is very close to the slightly time-delayed value, $\boldsymbol{H_i(t-\lambda)}$, where $\boldsymbol{\lambda}$ is small, then $\boldsymbol{H_i(t)}$ can be approximated by $\boldsymbol{H_i(t-\lambda)}$. Using the preceding equation, we then get a simplified method to compute $\hat{\boldsymbol{H}}_i(t)$:

$$\widehat{\boldsymbol{H}_i}(t) = \boldsymbol{H_i}(t-\lambda) = \tau_i(t-\lambda) - \bar{\boldsymbol{D}}_i\ddot{\boldsymbol{q}}_i(t-\lambda). \tag{8}$$

Since (8) does not involve $\boldsymbol{D_i(q_i)}$ and $\boldsymbol{E_i(q_i, \dot{q}_i)}$, it is robust with respect to robot model uncertainty. Equation (8) also does not include $\boldsymbol{J_i^T(q_i)\tilde{f}_i}$ and, thus, it is robust with respect to the effects of the object dynamics (or payload) which are accounted for by $\boldsymbol{J_i^T(q_i)\tilde{f}_i}$. The ideal result is obtained when $\boldsymbol{\lambda}$ is zero. In practice, $\boldsymbol{\lambda}$ is chosen as the sampling period. $\widehat{\boldsymbol{H}_i}$ requires joint acceleration measurements, $\ddot{\boldsymbol{q}}_i$, which are typically not available in practice. However, in many industrial robots the joint motor angular positions are measured by high-resolution optical encoders and it is feasible to compute $\ddot{\boldsymbol{q}}_i$ using finite difference algorithms. This technique introduces some noise [16], but has been successfully implemented [12].

Up to this point the control input, $\boldsymbol{u_i}$, is a joint-level control input. To transform to Cartesian space we use the following relationships

$$\dot{\boldsymbol{x}}_i = \boldsymbol{J_i(q_i)}\dot{\boldsymbol{q}}_i \tag{9}$$

$$\ddot{\boldsymbol{q}}_i = \boldsymbol{J_i^{-1}(q_i)}[\ddot{\boldsymbol{x}}_i - \dot{\boldsymbol{J}}_i\boldsymbol{(q_i, \dot{q}_i)}\dot{\boldsymbol{q}}_i] \tag{10}$$

to get

$$\boldsymbol{u_i} = \boldsymbol{J_i^{-1}(q_i)}(\nu_i - \dot{\boldsymbol{J}}_i\boldsymbol{(q_i, \dot{q}_i)}\dot{\boldsymbol{q}}_i) \tag{11}$$

which results in

$$\ddot{\boldsymbol{x}}_i = \boldsymbol{\nu_i}. \tag{12}$$

$\boldsymbol{\nu_i}$ is the Cartesian-space control to be designed for the *ith* manipulator and $\dot{\boldsymbol{x}}_i$ and $\ddot{\boldsymbol{x}}_i$ are the Cartesian velocity and acceleration, respectively.

As in [10], we design the control input, $\boldsymbol{\nu_i}$, by giving the properties of the following impedance to each manipulator where internal force is used in the relationship:

$$\boldsymbol{M_i}\delta\ddot{\boldsymbol{x}}_i + \boldsymbol{B_i}\delta\dot{\boldsymbol{x}}_i + \boldsymbol{K_i}\delta\boldsymbol{x_i} = \delta\tilde{\boldsymbol{f}}_{\boldsymbol{Ii}}. \tag{13}$$

$\boldsymbol{M_i}$, $\boldsymbol{B_i}$, and $\boldsymbol{K_i}$ are the desired inertia, damping, and stiffness matrices for the *ith* manipulator, $\delta\boldsymbol{x_i} = \boldsymbol{x_{id}} - \boldsymbol{x}$, and $\delta\tilde{\boldsymbol{f}}_{\boldsymbol{Ii}} = \tilde{\boldsymbol{f}}_{\boldsymbol{Ii}} - \tilde{\boldsymbol{f}}_{\boldsymbol{Iid}}$. The subscript d denotes a desired quantity. The internal force, $\tilde{\boldsymbol{f}}_{\boldsymbol{Ii}}$, is computed as in [17]:

$$\tilde{\boldsymbol{f}}_{\boldsymbol{Ii}} = \boldsymbol{P}_{\boldsymbol{Ii}}\tilde{\boldsymbol{f}} \tag{14}$$

where $\boldsymbol{P_{Ii}}$ are the $6i$-5 through $6i$ rows of $\boldsymbol{P_I}$ and

$$\boldsymbol{P_I} = \boldsymbol{I_{6n}} - \frac{\boldsymbol{1}}{\boldsymbol{n}}\begin{bmatrix} \boldsymbol{I_6} & \boldsymbol{J_{o1}^{-T}J_{o2}^T} & \cdots & \boldsymbol{J_{o1}^{-T}J_{on}^T} \\ \boldsymbol{J_{o2}^{-T}J_{o1}^T} & \boldsymbol{I_6} & \cdots & \boldsymbol{J_{o2}^{-T}J_{on}^T} \\ \vdots & \vdots & \ddots & \vdots \\ \boldsymbol{J_{on}^{-T}J_{o1}^T} & \boldsymbol{J_{on}^{-T}J_{o2}^T} & \cdots & \boldsymbol{I_6} \end{bmatrix}. \tag{15}$$

Each object-to-*ith*-manipulator Jacobian transpose is given by

$$\boldsymbol{J_{oi}^T} = \begin{bmatrix} & \boldsymbol{I_3} & & \boldsymbol{O_3} \\ \begin{bmatrix} \boldsymbol{0} & \boldsymbol{p_{iz}} & \boldsymbol{-p_{iy}} \\ \boldsymbol{-p_{iz}} & \boldsymbol{0} & \boldsymbol{p_{ix}} \\ \boldsymbol{p_{iy}} & \boldsymbol{-p_{ix}} & \boldsymbol{0} \end{bmatrix} & & & \boldsymbol{I_3} \end{bmatrix} \tag{16}$$

where $\boldsymbol{p_i} = [\boldsymbol{p_{ix}}\ \boldsymbol{p_{iy}}\ \boldsymbol{p_{iz}}]^{\boldsymbol{T}}$ is the vector from the *ith* end effector to the object frame as shown in Figure 1.

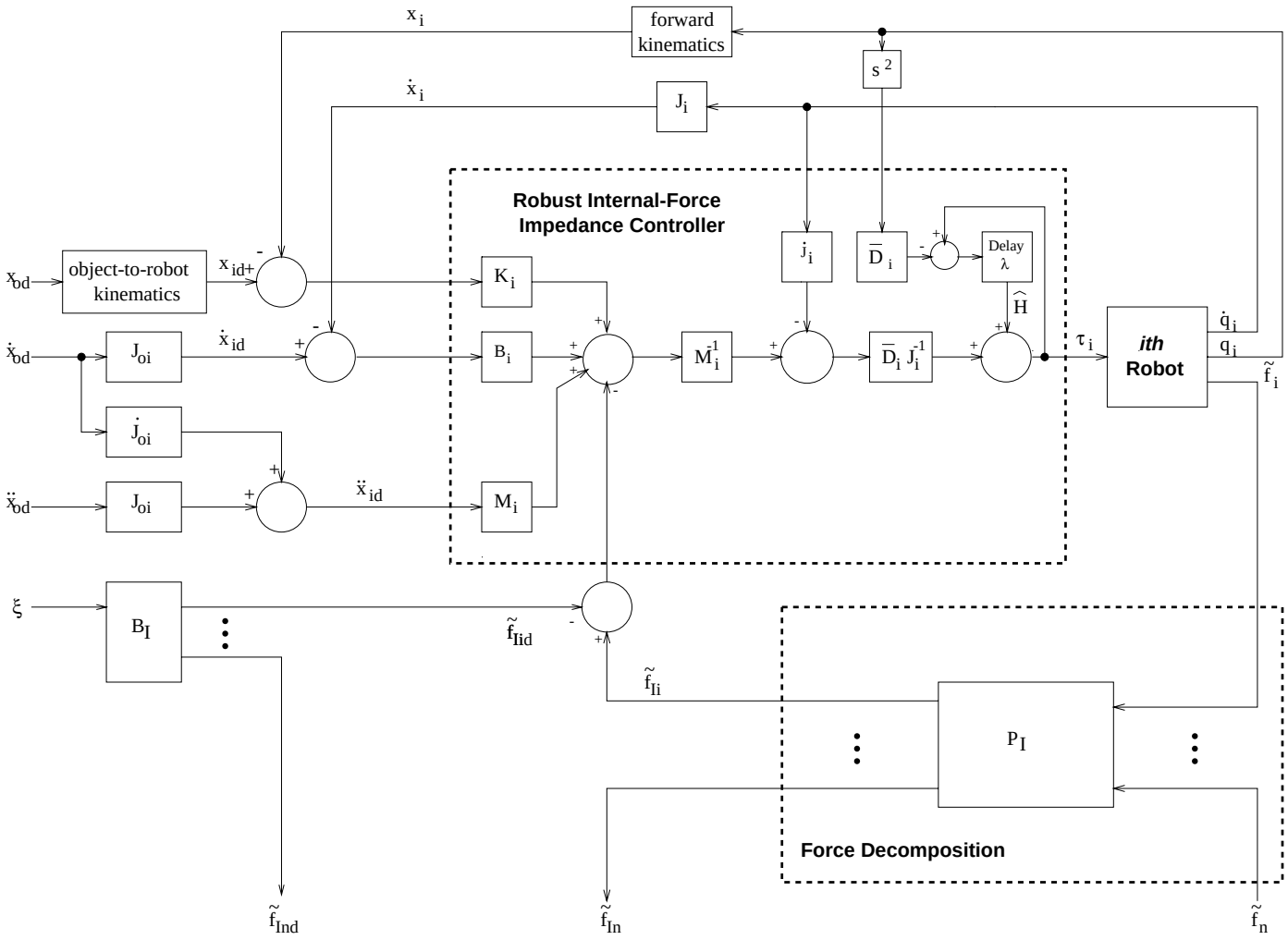

Fig. 2. Controller

The desired internal force must be chosen to lie in the range of the internal force projection operator, $\boldsymbol{P_I}$, which is rank $6n$-6 [10]. That is, $\tilde{\boldsymbol{f}}_{\boldsymbol{Id}} = [\tilde{\boldsymbol{f}}_{\boldsymbol{I1d}}^{\boldsymbol{T}}\ \tilde{\boldsymbol{f}}_{\boldsymbol{I2d}}^{\boldsymbol{T}} \cdots \tilde{\boldsymbol{f}}_{\boldsymbol{Ind}}^{\boldsymbol{T}}]^{\boldsymbol{T}} = \boldsymbol{B_I}\boldsymbol{\xi}$ where $\boldsymbol{B_I}$ is a basis for $\boldsymbol{P_I}$ and $\boldsymbol{\xi}$ is a ($6n$-6)x1 vector which parameterizes the desired internal force. For example, for n=2 a basis for $\boldsymbol{P_I}$ is

$$\boldsymbol{B_I} = \begin{bmatrix} -\boldsymbol{J}_{\boldsymbol{o1}}^{-\boldsymbol{T}} \\ \boldsymbol{J}_{\boldsymbol{o2}}^{-\boldsymbol{T}} \end{bmatrix}. \tag{17}$$

Then $\boldsymbol{\xi}$ represents the internal force as seen at the object frame and the desired internal force at the end effectors is $\tilde{\boldsymbol{f}}_{\boldsymbol{I1d}} = -\boldsymbol{J}_{\boldsymbol{o1}}^{-\boldsymbol{T}}\boldsymbol{\xi}$ and $\tilde{\boldsymbol{f}}_{\boldsymbol{I2d}} = \boldsymbol{J}_{\boldsymbol{o2}}^{-\boldsymbol{T}}\boldsymbol{\xi}$.

Solving (13) for $\ddot{\boldsymbol{x}}_{\boldsymbol{i}}$ and substituting into (12) yields the following Cartesian-space control input:

$$\boldsymbol{\nu_i} = \ddot{\boldsymbol{x}}_{\boldsymbol{id}} + \boldsymbol{M}_{\boldsymbol{i}}^{-\boldsymbol{1}}(\boldsymbol{B}_{\boldsymbol{i}}\boldsymbol{\delta}\dot{\boldsymbol{x}}_{\boldsymbol{i}} + \boldsymbol{K}_{\boldsymbol{i}}\boldsymbol{\delta}\boldsymbol{x}_{\boldsymbol{i}} - \boldsymbol{\delta}\tilde{\boldsymbol{f}}_{\boldsymbol{Ii}}). \tag{18}$$

Finally, combining (6), (11) and (18), we get the following robust internal force-based impedance control law:

$$\boldsymbol{\tau_i} = \bar{\boldsymbol{D}}_{\boldsymbol{i}}\{\boldsymbol{J}_{\boldsymbol{i}}^{-\boldsymbol{1}}[\boldsymbol{M}_{\boldsymbol{i}}^{-\boldsymbol{1}}(\boldsymbol{M}_{\boldsymbol{i}}\ddot{\boldsymbol{x}}_{\boldsymbol{id}} + \boldsymbol{B}_{\boldsymbol{i}}\boldsymbol{\delta}\dot{\boldsymbol{x}}_{\boldsymbol{i}} + \boldsymbol{K}_{\boldsymbol{i}}\boldsymbol{\delta}\boldsymbol{x}_{\boldsymbol{i}} - \boldsymbol{\delta}\tilde{\boldsymbol{f}}_{\boldsymbol{Ii}}) - \dot{\boldsymbol{J}}_{\boldsymbol{i}}\dot{\boldsymbol{q}}_{\boldsymbol{i}}]\} + \widehat{\boldsymbol{H}}_{\boldsymbol{i}}. \tag{19}$$

$\widehat{\boldsymbol{H}}_{\boldsymbol{i}}$ compensates for both the manipulator and object dynamics and, thus, the control law (19) is robust with respect to payload variations in addition to robot model uncertainty. Furthermore, since internal force is used in the impedance relationship, the object dynamics do not contribute to tracking and steady-state position errors. The controller is depicted in Figure 2.

B. Stability Analysis

The stability of control systems using the estimate $\widehat{\boldsymbol{H}}_{\boldsymbol{i}}$ was studied for joint-space and unconstrained Cartesian-space control schemes in [13], [11]. The stability analysis in [13] relies on some reasonable assumptions of the continuity of the manipulator dynamics and defines a representation of the estimation error of $\boldsymbol{H_i(t)}$ by $\widehat{\boldsymbol{H}}_{\boldsymbol{i}}\boldsymbol{(t)}$ for the *ith* manipulator to be

$$\boldsymbol{\epsilon_i(t) = \bar{D}_i^{-1}[H_i(t-\lambda) - H_i(t)].} \tag{20}$$

Combining (4), (6), (8), (11), (18), and the preceding equation, yields the closed-loop system error equation:

$$\boldsymbol{M_i\delta\ddot{x}_i + B_i\delta\dot{x}_i + K_i\delta x_i = \delta f_{Ii} - M_iJ_i\epsilon_i.} \tag{21}$$

When $\boldsymbol{\epsilon_i = 0}$ (i.e., $\boldsymbol{\lambda = 0}$), so does $\boldsymbol{M_iJ_i\epsilon_i}$ since $\boldsymbol{M_iJ_i}$ is bounded. This is equivalent to having an exact dynamic model and exactly canceling the nonlinear dynamics as in a computed-torque control law which was previously shown to be stable for rigid grasping if each $\boldsymbol{M_i}$, $\boldsymbol{B_i}$, and $\boldsymbol{K_i}$ is symmetric positive definite and each robot's Jacobian, $\boldsymbol{J_i}$, is nonsingular [10].

When $\boldsymbol{\epsilon_i \neq 0}$, $\boldsymbol{M_iJ_i\epsilon_i}$ can be considered an additional forcing function and the system (21) will have bounded-input bounded-output (BIBO) stability if $\boldsymbol{\epsilon_i}$ is bounded since $\boldsymbol{M_iJ_i}$ is bounded. It was shown in [13] that

$$\boldsymbol{\epsilon_i(t) = [I - D_i^{-1}(t)\bar{D}_i]\epsilon_i(t-\lambda) + R_i(t,\lambda)} \tag{22}$$

where $\boldsymbol{R_i(t,\lambda)}$ is a continuous function of the *ith* manipulator dynamics and is bounded. The unforced part of the preceding equation is $\boldsymbol{\epsilon_i(t) = [I - D_i^{-1}(t)\bar{D}_i]\epsilon_i(t-\lambda)}$ which, for digital implementation, can be approximated by

$$\boldsymbol{\epsilon_i(k) = [I - D_i^{-1}(k)\bar{D}_i]\epsilon_i(k-1)} \tag{23}$$

where k is the sample instant.

The system (23) is asymptotically stable if the eigenvalues of $\boldsymbol{[I - D_i^{-1}(k)\bar{D}_i]}$ lie within the unit circle on the z-plane. In [13] it was shown that the condition is met if $\boldsymbol{\bar{D}_i}$ is chosen as $\boldsymbol{\bar{D}_i = \alpha_i I}$ where $\boldsymbol{\alpha_i}$ is a scaler constant and $\boldsymbol{0 < \alpha_i < 2\rho_i}$ where $\boldsymbol{\rho_i}$ is the minimum eigenvalue of the actual manipulator inertia matrix, $\boldsymbol{D_i(q_i)}$. Thus, $\boldsymbol{0 < \alpha_i < 2\rho_i}$ is a necessary condition for stability, but there may be other conditions since $\boldsymbol{\epsilon_i}$ is a function of $\boldsymbol{q}$, $\boldsymbol{\dot{q}}$, and the control signal and, thus, it is not independent of the left-hand side of (21). Extensive simulations in [13] indicate that it is a primary stability condition.

C. The Design of $\bar{\boldsymbol{D}}_{\boldsymbol{i}}$

The control law (19) requires the design of $\boldsymbol{\bar{D}_i}$ for each manipulator. In [13] it was shown that if $\boldsymbol{0 < \alpha_i < 2\rho_i}$ is met under no load conditions, it will also be satisfied with added payload. Furthermore, a method to experimentally determine $\boldsymbol{\alpha_i}$ was presented so that one can determine $\boldsymbol{\bar{D}_i}$ in the absence of a robot model.

Examination of $\boldsymbol{I - D_i^{-1}(k)\bar{D}_i}$ reveals that the closer $\boldsymbol{\bar{D}_i}$ is to the actual manipulator inertia, $\boldsymbol{D_i}$, the closer the poles of $\boldsymbol{I - D_i^{-1}(k)\bar{D}_i}$ are to the z-plane origin and the faster the convergence of $\boldsymbol{\epsilon(k)}$ to zero, or $\widehat{\boldsymbol{H}}_{\boldsymbol{i}}$ to $\boldsymbol{H_i}$. Thus, if one does have knowledge of the manipulator inertia matrix, it behooves one to choose $\boldsymbol{\bar{D}_i}$ close to $\boldsymbol{D_i}$. For example, the PUMA 560 manipulator is highly geared and its inertia matrix is diagonally dominant and from [18] one could choose $\boldsymbol{\bar{D}_i = diag\{2.57\ 6.79\ 1.16\ 0.2\ 0.19\ 0.18\}}$ to achieve faster convergence than $\boldsymbol{\bar{D}_i = \alpha_i I}$.

III. Computational Delays

A. Single Manipulator

Before analyzing in detail the effects of computational delays on the multi-arm system, their effects are examined for a single impedance-controlled manipulator with its environment in which the control law is implemented digitally. We

will assume that the manipulator motion is completely constrained. One may question the validity of examining such a restrictive situation, but the analysis may be applied to the case of the manipulator in contact with a rigid surface. Once the manipulator breaks contact, then the manipulator is operating in free space and the impedance law is equivalent to PD control. While in contact with a completely rigid surface, the analysis of this section applies.

During single-arm operation, the control law becomes

$$\boldsymbol{\tau = \bar{D}\{J^{-1}[M^{-1}(M\ddot{x}_d + B\delta\dot{x} + K\delta x - \delta\tilde{f}) - \dot{J}\dot{q}]\} + \widehat{H}.} \tag{24}$$

where $\boldsymbol{\delta\tilde{f}_I}$ has been replaced by the total force error $\boldsymbol{\delta\tilde{f}}$. During unconstrained operation, there is no environment to impose a force on the end effector and, therefore, $\boldsymbol{\delta\tilde{f} = 0}$.

The effect of computational delays on the constrained single-arm impedance controlled manipulator is stated as the following theorem:

Theorem 1: A constrained manipulator employing a digital implementation of control law (24) is exponentially stable if: 1) $\boldsymbol{J}$ is non-singular, 2) $\boldsymbol{M}$ is chosen such that the magnitude of each of the eigenvalues of $\boldsymbol{I_6 - J^{-T}\bar{D}J^{-1}M^{-1}}$ is less than one, and 3) $\boldsymbol{\delta x = 0}$.

Proof. The last condition does not affect the stability results because if it is not met, then the only effect is to add a constant amount, $\boldsymbol{K\delta x}$, to the desired force. It is added as a condition to simplify the analysis. Substituting the control law (24) into the dynamic equation for the manipulator (2), yields

$$\boldsymbol{\bar{D}\ddot{q} + H = \bar{D}\{J^{-1}[M^{-1}(M\ddot{x}_d + B\delta\dot{x} + K\delta x - \delta\tilde{f}) - \dot{J}\dot{q}]\} + \widehat{H}} \tag{25}$$

In the constrained case, the manipulator is not moving and, thus, $\boldsymbol{\dot{q} = \ddot{q} = \delta x = \delta\dot{x} = \ddot{x}_d = 0}$ and $\boldsymbol{D}$, $\boldsymbol{E}$, and $\boldsymbol{J}$ are constant. Equation (25) reduces to

$$\boldsymbol{J^T\tilde{f} = -\bar{D}J^{-1}M^{-1}\delta\tilde{f} + J^T\tilde{f}.} \tag{26}$$

For the digital case, it is observed that when the left side of equation (26) is at sample instant k+1, the right side (the control input) is at sample instant k due to the one-sample delay inherent in the digital controller. Equation (26) becomes the following discrete-time equation:

$$\boldsymbol{J^T\tilde{f}_{k+1} = -\bar{D}J^{-1}M^{-1}\delta\tilde{f}_k + J^T\tilde{f}_k} \tag{27}$$

which results in

$$\boldsymbol{\tilde{f}_{k+1} = (I_6 - J^{-T}\bar{D}J^{-1}M^{-1})\tilde{f}_k + J^{-T}\bar{D}J^{-1}M^{-1}\tilde{f}_{dk} = \Phi_{cl}\tilde{f}_k + \Gamma\tilde{f}_{dk}.} \tag{28}$$

Equation (28) describes the dynamics of the constrained manipulator system. The stability of the discrete system (28) is determined by the eigenvalues of $\boldsymbol{\Phi_{cl}}$. The system is exponentially stable if $\boldsymbol{M}$ is chosen such that the eigenvalues of $\boldsymbol{\Phi_{cl}}$ are all less than one in magnitude. Equation (28) also requires that $\boldsymbol{J}$ be non-singular. Thus, the necessity for condition 1. □

The term $\boldsymbol{J^{-T}\bar{D}J^{-1}}$ is the estimated approximate Cartesian inertia of the manipulator as seen at the end effector. Theorem 1 places a bound on how much smaller the desired inertia, $\boldsymbol{M}$, can be relative to the estimated Cartesian end-point inertia of the manipulator. The bound is independent of the sample time. This independence is an artifact of assuming that the manipulator is completely rigid and constrained.

B. Dual-arm System

In a dual-arm system, each manipulator interacts with the object and the other manipulator and its motion is constrained by kinematic relationships. To determine the effect of computational delays, we will assume that the manipulators and the object are completely constrained. This is analogous to having the held object in contact with a

rigid surface. Although not the most general case, it does yield insight into the control of internal forces in the system. Without this assumption the problem is less mathematically tractable. While the analysis is not directly applicable to the unconstrained case, the results have been conservative in simulations studies and should yield sufficient conditions for stability for the unconstrained system.

The effect of computational delays on the constrained dual-arm system is stated as the following theorem:

Theorem 2: A constrained dual-arm system where each manipulator rigidly grasps the other and where each manipulator employs a digital implementation of control law (19) is BIBO stable if: 1) each $\boldsymbol{J_i}$ is non-singular, 2) each $\boldsymbol{M_i}$, is chosen such that the magnitude of each of the eigenvalues of $\left[\boldsymbol{I_6} - \frac{1}{2}\boldsymbol{J_{o1}^T J_1^{-T} \bar{D}_1 J_1^{-1} M_1^{-1} J_{o1}^{-T}} - \frac{1}{2}\boldsymbol{J_{o2}^T J_2^{-T} \bar{D}_2 J_2^{-1} M_2^{-1} J_{o2}^{-T}}\right]$ is less than one, and 3) $\boldsymbol{\delta x_i = 0}$ for i=1,2.

Proof. As in the single arm case, the last condition does not affect the stability results because if it is not met, then the only effect is to add a constant amount, $\boldsymbol{K_i \delta x_i}$, to the desired internal force. It is added as a condition to simplify the analysis. Substituting the control law (19) into the dynamic equation for the *ith* manipulator (2), yields

$$\boldsymbol{\bar{D}_i \ddot{q}_i + H_i = \bar{D}_i\{J_i^{-1}[M_i^{-1}(M_i \ddot{x}_{id} + B_i \delta \dot{x}_i + K_i \delta x_i - \delta \tilde{f}_{Ii}) - \dot{J}_i \dot{q}_i]\} + \widehat{H}_i.} \tag{29}$$

In the constrained case, the manipulators are not moving and, thus, $\boldsymbol{\dot{q}_i = \ddot{q}_i = \delta x_i = \delta \dot{x}_i = \ddot{x}_{id} = 0}$ and $\boldsymbol{D_i}$, $\boldsymbol{E_i}$, and $\boldsymbol{J_i}$ are constant. The preceding equation reduces to

$$\boldsymbol{J_i^T \tilde{f}_i = -\bar{D}_i J_i^{-1} M_i^{-1} \delta \tilde{f}_{Ii} + J_i^T \tilde{f}_i.} \tag{30}$$

For the digital case, it is observed that when the left side of equation (30) is at sample instant k+1, the right side (the control input) is at sample instant k due to the one sample delay inherent in the digital controller. Equation (30) becomes the following discrete-time equation:

$$\boldsymbol{J_i^T \tilde{f}_{i(k+)} = -\bar{D}_i J_i^{-1} M_i^{-1} \delta \tilde{f}_{Iik} + J_i^T \tilde{f}_{ik}} \tag{31}$$

which results in

$$\boldsymbol{\tilde{f}_{i(k+1)} = \tilde{f}_{ik} - J_i^{-T} \bar{D}_i J_i^{-1} M_i^{-1} \tilde{f}_{Iik} + J_i^{-T} \bar{D}_i J_i^{-1} J_i^{-1} \tilde{f}_{Iidk}.} \tag{32}$$

Using the definition of internal force from (14), we get

$$\boldsymbol{\tilde{f}_{I1k} = \frac{1}{2}(\tilde{f}_{1k} - J_{o1}^{-T} J_{o2}^T \tilde{f}_{2k})} \quad \text{and}$$
$$\boldsymbol{\tilde{f}_{I2k} = \frac{1}{2}(\tilde{f}_{2k} - J_{o2}^{-T} J_{o1}^T \tilde{f}_{1k}).} \tag{33}$$

Substituting (33) into (32) yields

$$\begin{bmatrix} \tilde{f}_{1(k+1)} \\ \tilde{f}_{2(k+1)} \end{bmatrix} = \begin{bmatrix} I_6 - \frac{1}{2}J_1^{-T}\bar{D}_1 J_1^{-1} M_1^{-1} & \frac{1}{2}J_1^{-T}\bar{D}_1 J_1^{-1} M_1^{-1} J_{o1}^{-T} J_{o2}^T \\ \frac{1}{2}J_2^{-T}\bar{D}_2 J_2^{-1} M_2^{-1} J_{o2}^{-T} J_{o1}^T & I_6 - \frac{1}{2}J_2^{-T}\bar{D}_2 J_2^{-1} M_2^{-1} \end{bmatrix} \begin{bmatrix} \tilde{f}_{1k} \\ \tilde{f}_{2k} \end{bmatrix} + \begin{bmatrix} J_1^{-T}\bar{D}_1 J_1^{-1} M_1^{-1} \\ -J_2^{-T}\bar{D}_2 J_2^{-1} M_2^{-1} J_{o2}^{-T} J_{o1}^T \end{bmatrix} \tilde{f}_{I1dk} \tag{34}$$

or

$$\boldsymbol{\tilde{f}_{k+1} = A\tilde{f}_k + \begin{bmatrix} B_1 \\ B_2 \end{bmatrix} \tilde{f}_{I1dk} = A\tilde{f}_k + B\tilde{f}_{I1dk}.} \tag{35}$$

Using the PBH rank test [19], we find that the system $\boldsymbol{(A, B)}$ is not completely reachable. We use the following transformation to decompose the system $\boldsymbol{(A, B)}$ into its reachable and unreachable parts:

$$\boldsymbol{T = \begin{bmatrix} 2(I_6 - J_{o1}^{-T} J_{o2}^T \Delta^{-1} B_1^{-1}) J_{o1}^{-T} & J_{o1}^{-T} J_{o2}^T \Delta^{-1} \\ -2\Delta^{-1} B_1^{-1} J_{o1}^{-T} & \Delta^{-1} \end{bmatrix}} \tag{36}$$

where $\boldsymbol{\Delta = B_1^{-1} J_{o1}^{-T} J_{o2}^T - B_2^{-1}}$. The transformed system matrices and state vector are

$$\hat{\boldsymbol{A}} = \boldsymbol{T}^{-1}\boldsymbol{A}\boldsymbol{T} = \begin{bmatrix} \hat{\boldsymbol{A}}_{11} & \hat{\boldsymbol{A}}_{12} \\ \hat{\boldsymbol{A}}_{21} & \hat{\boldsymbol{A}}_{22} \end{bmatrix} = \begin{bmatrix} \boldsymbol{I}_6 - \frac{1}{2}\boldsymbol{J}_{o1}^T\boldsymbol{B}_1\boldsymbol{J}_{o1}^{-T} + \frac{1}{2}\boldsymbol{J}_{o2}^T\boldsymbol{B}_2\boldsymbol{J}_{o1}^{-T} & \boldsymbol{0}_6 \\ \boldsymbol{0}_6 & \boldsymbol{I}_6 \end{bmatrix} \tag{37}$$

$$\hat{\boldsymbol{B}} = \boldsymbol{T}^{-1}\boldsymbol{B} = \begin{bmatrix} \hat{\boldsymbol{B}}_1 \\ \hat{\boldsymbol{B}}_2 \end{bmatrix} = \begin{bmatrix} \frac{1}{2}\boldsymbol{J}_{o1}^T\boldsymbol{B}_1 - \frac{1}{2}\boldsymbol{J}_{o2}^T\boldsymbol{B}_2 \\ \boldsymbol{0}_6 \end{bmatrix} \tag{38}$$

$$\hat{\boldsymbol{f}}_k = \boldsymbol{T}^{-1}\tilde{\boldsymbol{f}}_k = \begin{bmatrix} \hat{\boldsymbol{f}}_{1k} \\ \hat{\boldsymbol{f}}_{2k} \end{bmatrix} = \begin{bmatrix} \boldsymbol{J}_{o1}^T\tilde{\boldsymbol{f}}_{I1k} \\ \boldsymbol{B}_1^{-1}\tilde{\boldsymbol{f}}_{1k} - \boldsymbol{B}_2^{-1}\tilde{\boldsymbol{f}}_{2k} \end{bmatrix}. \tag{39}$$

The reachable part of the state, $\hat{\boldsymbol{f}}_{1k}$, is the internal force exerted by manipulator 1 at the origin of the object frame. It is characterized by

$$\hat{\boldsymbol{f}}_{1(k+1)} = \hat{\boldsymbol{A}}_{11}\hat{\boldsymbol{f}}_{1k} + \hat{\boldsymbol{B}}_1\tilde{\boldsymbol{f}}_{I1dk}. \tag{40}$$

The unreachable part is described by $\hat{\boldsymbol{f}}_{2(k+1)} = \hat{\boldsymbol{f}}_{2k}$.

The stability of the reachable part is governed by the eigenvalues of $\hat{\boldsymbol{A}}_{11}$. If its eigenvalues are less than one in magnitude, the reachable part is asymptotically stable. The unreachable part has all its eigenvalues equal to one and, therefore, is stable in the sense of Lyapunov, but not asymptotically stable. The LTI system $(\hat{\boldsymbol{A}}, \hat{\boldsymbol{B}})$ or $(\boldsymbol{A}, \boldsymbol{B})$ is BIBO stable if $\boldsymbol{M}_1$ and $\boldsymbol{M}_2$ are chosen such that the eigenvalues of the reachable part are less than one in magnitude. Equation (40) also requires that $\boldsymbol{J}_i$ be non-singular. Thus, the necessity for condition 1. □

Theorem 2 places a lower bound on the size of $\boldsymbol{M}_i$ with respect to each manipulator's estimated Cartesian end-point inertia which is independent of the sample time (again, an artifact of the rigidity and constraint assumptions). The unreachable part represents the sum of the forces exerted by both manipulators as if each had inertia, $\boldsymbol{M}_i$. The unreachable part of the system $(\hat{\boldsymbol{A}}, \hat{\boldsymbol{B}})$ is an expression of the principle that we cannot simultaneously control both the position of and the net force on the object. In control law (19) we control the position of the object and the internal force which is the reachable part.

IV. Experimental Setup

The UCD Robotics Research Laboratory (RRL) experimental testbed consists of two PUMA 560 industrial manipulators fitted with JR3 wrist force sensors. Each manipulator is controlled by a UCD RRL-designed controller (Figure 3) consisting of: 1) a 486 personal computer; 2) electronics (located in the 486 or Multibus chassis) to read the voltages from the joint potentiometers, to read each joint's digital encoder signals, and to output control signals to the Unimate motor voltage amplifiers; 3) a force sensor interface card; 4) a TMS320C30/C40 DSP board; and 5) a GPIB interface board.

The UCD controller software (Figure 4) which provides the capability for real-time control of the PUMA manipulators consists of: 1) a controller device driver which provides the interrupt service routine and communicates with the hardware, the GPIB driver and the DSP board; 2) a GPIB device driver which provides inter-PC communications; 3) a DSP control program which does most of the control algorithm computations; and 4) applications programs which provide the operator interface.

The philosophy behind operation in the dual-arm mode is that the control functions should be distributed to the maximum extent possible between the controllers. Either controller can be designated as the "master" which is the computer through which the high-level commands are issued by the operator. Synchronization between the two controllers is accomplished by shutting off the interrupt source of the controller designated as the slave. The slave controller waits

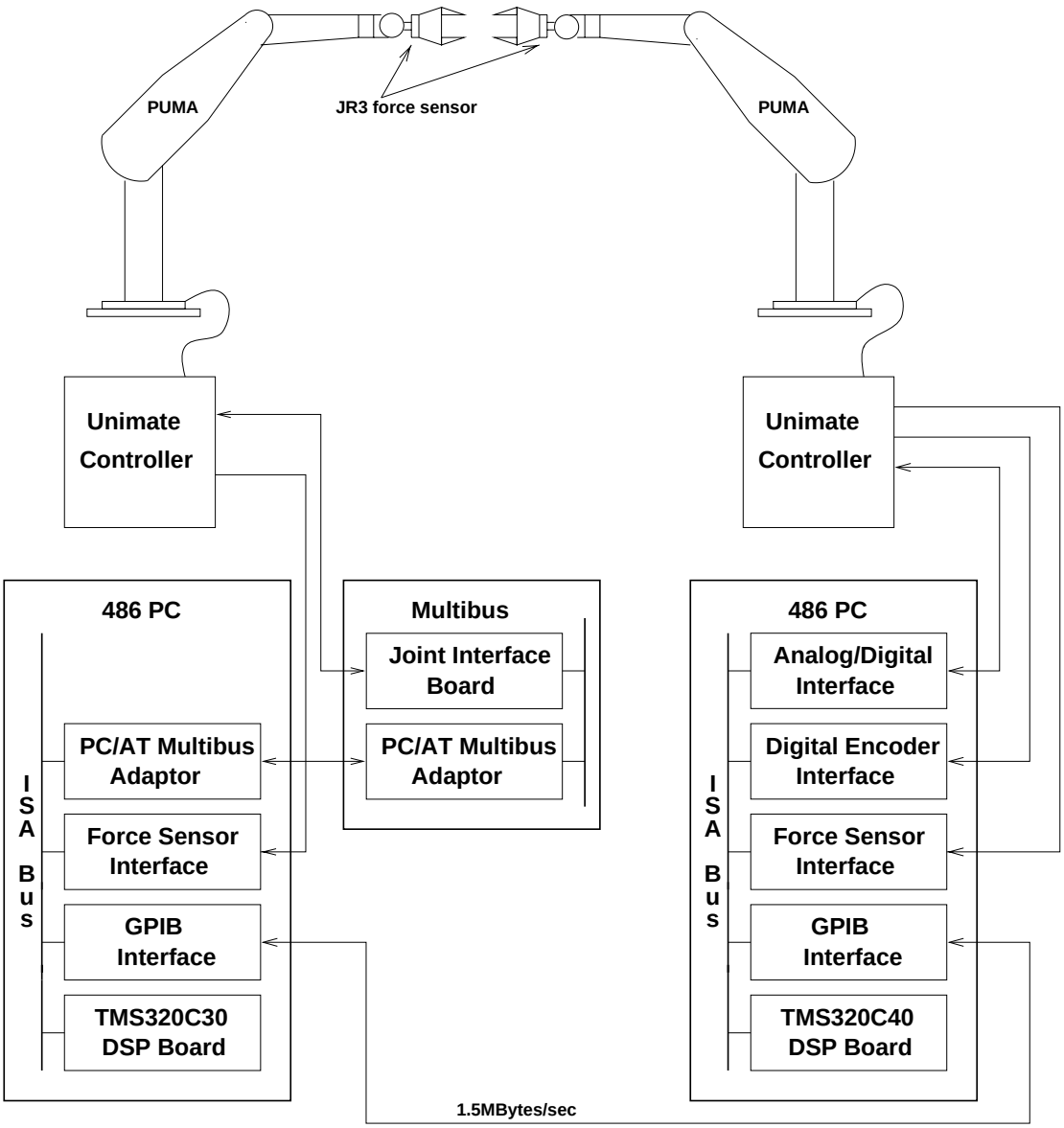

Fig. 3. UCD RRL Dual-Arm Testbed

for a signal from the master controller to start its control cycle. During each control cycle, force and transformation data is exchanged. When the user enters the command to return to the single-arm mode, the GPIB link is closed and the slave interrupt source is turned back on. The current sampling rate is 200Hz.

V. Experimental Results

For each of the experiments conducted below, the damping and stiffness matrices were chosen as $\boldsymbol{B_i = 62.9 M_i}$, and $\boldsymbol{K_i = 631 M_i}$ so that the bandwidth is the same for any choice of $\boldsymbol{M_i}$. Furthermore, in the dual-arm experiments the impedance chosen for each manipulator was identical. $\bar{\boldsymbol{D}}_{\boldsymbol{i}}$ was chosen to be diagonal as in section II-C except that the first element was reduced by 50% based on experimental data. The sampling period is 5 msec. Endpoint (single arm) or internal (dual arm) force and moment are plotted along with position and orientation errors for each experiment. The orientation error is expressed as the magnitude of the axis-angle representation of the error.

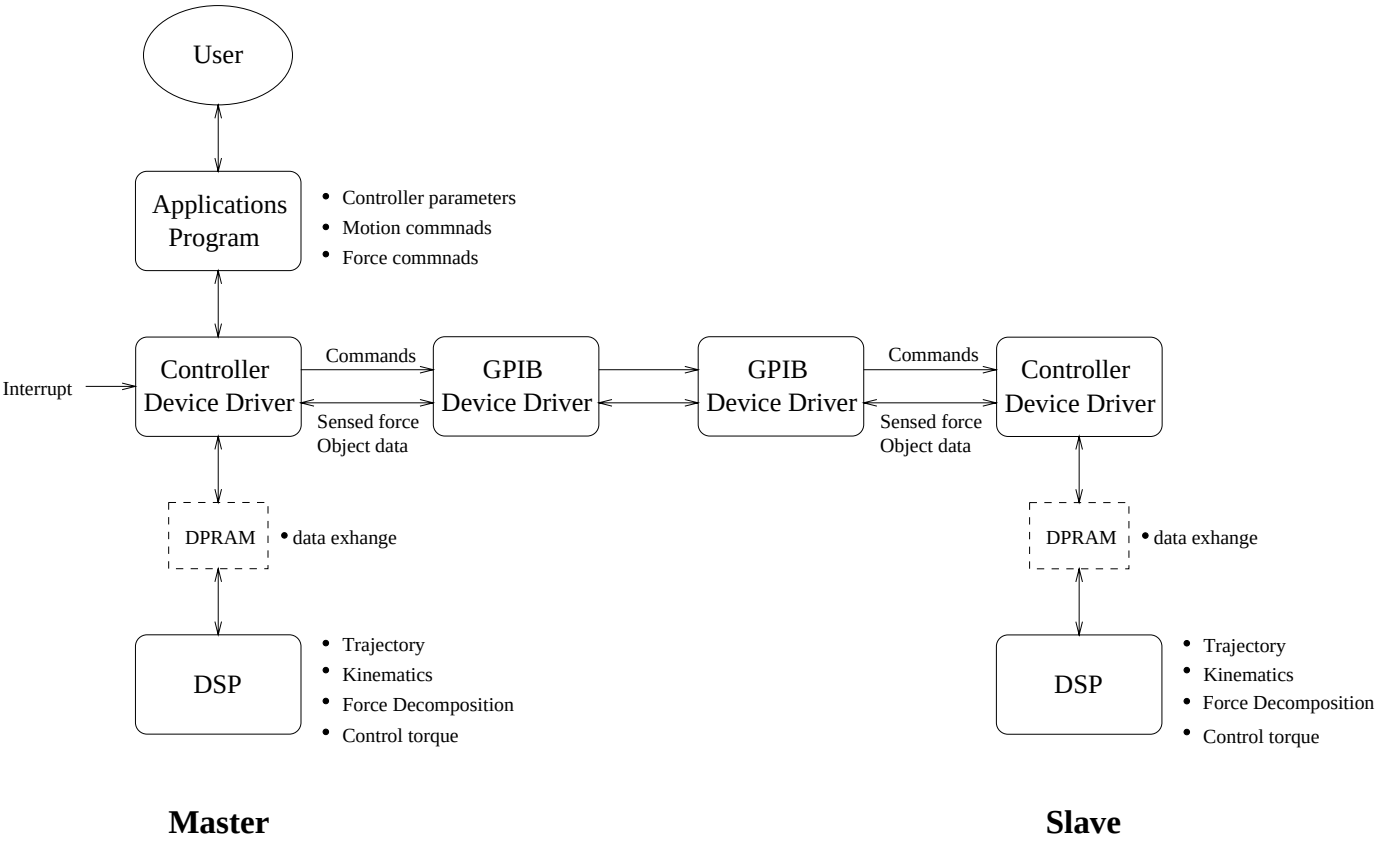

Fig. 4. UCD RRL Dual-arm Controller Software

A. Computational Delays - Single-arm

To test Theorem 1, a PUMA 560 was fitted with an end effector consisting of a rigid aluminum rod with a ball tip. The tip was brought into contact with a rigid surface located in the x-y plane and a 20N force step command given in the negative z direction as shown in Figure 5. The inertia matrix was chosen as $\boldsymbol{M = \kappa J^{-T} \bar{D} J^{-1}}$ with $\boldsymbol{\kappa = 0.9,\ 1.0,\ 2.0}$. Results of the experiments are shown in Figures 7-9. The amount of oscillatory behavior is inversely proportional to $\boldsymbol{\kappa}$. This is consistent with the theory. The lower bound is approximately $\boldsymbol{\kappa = 0.8}$ at which point a limit cycle occurs whereby the manipulator bounces on the surface. This value is somewhat higher than the theoretically predicted value of $\boldsymbol{\kappa = 0.5}$.

The experiments were repeated with diagonal $\boldsymbol{M}$ with separate translational and rotational components - $\boldsymbol{M = diag\{m_1 I_3,\ m_2 I_3\}}$. The theoretical lower bound on $\boldsymbol{M}$ was found to be $\boldsymbol{m_1 = 36}$ Kg and $\boldsymbol{m_2 = 1.3}$ Kg-m^2. Experiments were conducted for the following values of $\boldsymbol{(m_1, m_2)}$: $\boldsymbol{(23, .8)}$, $\boldsymbol{(36, 1.3)}$, $\boldsymbol{(50, 1.8)}$. The results are shown in Figures 10-12. As in the previous experiments, increasing $\boldsymbol{M}$ has a stabilizing influence on the force response and the response becomes less oscillatory as $\boldsymbol{M}$ increases. The experimental lower bound was $\boldsymbol{(m_1, m_2) = (23, .8)}$ which is somewhat lower than the theoretical, but the fundamental point that a lower bound exists is verified by the experiments.

B. Computational Delays - Dual-arm System

To test Theorem 2 a rigid object consisting of a .38m long stiff aluminum rod was bolted directly to the force sensors attached to two PUMA 560s as shown in Figure 6. For each experiment an internal force step command of $\boldsymbol{\xi = [20\ 0\ 0\ 0\ 0\ 0]}$N was issued. In the experimental plots, $\boldsymbol{\xi}$ is expressed in object-frame coordinates, but note that

it is expressed in world-frame coordinates when used to compute $\tilde{\boldsymbol{f}}_{\boldsymbol{Id}}$. The object frame is located at the center of the object with the x-axis pointed along the rod's long axis.

Experiments were conducted for each $\boldsymbol{M_i = \kappa J_i^{-T} \bar{D}_i J_i^{-1}}$ with $\boldsymbol{\kappa = 0.9,\ 1.0,\ 2.0}$. Results of the experiments are plotted in Figures 13-15. In each case the internal force at the object frame expressed in object-frame coordinates is plotted. The amount of oscillatory behavior is inversely proportional to $\boldsymbol{\kappa}$. Larger values of $\boldsymbol{\kappa}$ have a stabilizing influence on the force response. This is consistent with the theory. The lower bound is approximately $\boldsymbol{\kappa = 0.9}$ at which point the system goes unstable. The experimental value for the boundary is somewhat higher than the theoretically predicted value of $\boldsymbol{\kappa = 0.5}$.

The experiments were repeated for diagonal $\boldsymbol{M_i}$ using separate inertias for the translation and rotational components. The theoretical lower bound for the inertia is $\boldsymbol{(m_1, m_2) = (18, 0.6)}$. Experiments were conducted for the following $\boldsymbol{(m_1, m_2)}$: $\boldsymbol{(11, 0.4)}$, $\boldsymbol{(18, 0.6)}$, $\boldsymbol{(37, 1.3)}$. The results are plotted in Figures 16-18. The amount of oscillatory behavior is again inversely proportional to the inertia. Below $\boldsymbol{(m_1, m_2) = (11, 0.4)}$, the system is unstable. As with the single-arm case, the experimental lower bound for the inertia is somewhat lower than the theoretical bound.

Possible explanations for the deviation of the lower bound of the inertia from the theoretically predicted values for both the single and dual-arm cases are that neither manipulator is truly rigid and the noncolocation of the force sensors and actuators along with possibly other nonlinear effects may contribute to instability. Even though the experimental and theoretical values do not match exactly, they are close and the experiments verify that there is a lower bound on the inertia matrix and that appropriate choice of each $\boldsymbol{M_i}$ has a stabilizing influence on the force response.

C. Trajectory Tracking

To test the tracking capability of the control law presented in section II-A, motion experiments were conducted with the robots manipulating the rigid object. Based on the results of the preceding section, each impedance inertia was chosen as $\boldsymbol{M_i = 2 J_i^{-T} \bar{D}_i J_i^{-1}}$.

The object frame was chosen to be the geometric center of the object and the right PUMA base frame designated as the world frame. The trajectory for the motion experiments is based on a fifth-order polynomial. To compute the orientation trajectory the desired rotation matrix is first converted to a quaternion, the interpolation done, and then the quaternion set point converted back into the desired rotation matrix. Each controller computes its own trajectory on line from the desired object set point.

The motion experiment consisted of moving the object from

$$ {}^{w}\boldsymbol{T}_{obj} = \begin{bmatrix} \mathbf{1} & \mathbf{0} & \mathbf{0} & \mathbf{.650} \\ \mathbf{0} & \mathbf{1} & \mathbf{0} & \mathbf{.150} \\ \mathbf{0} & \mathbf{0} & \mathbf{1} & \mathbf{.450} \\ \mathbf{0} & \mathbf{0} & \mathbf{0} & \mathbf{1} \end{bmatrix} \tag{41} $$

to

$$ {}^{w}\boldsymbol{T}_{obj} = \begin{bmatrix} \mathbf{0.958} & \mathbf{0} & \mathbf{0.287} & \mathbf{.800} \\ \mathbf{0} & \mathbf{1} & \mathbf{0} & \mathbf{.150} \\ \mathbf{-0.287} & \mathbf{0} & \mathbf{0.958} & \mathbf{.250} \\ \mathbf{0} & \mathbf{0} & \mathbf{0} & \mathbf{1} \end{bmatrix} \tag{42} $$

in two seconds with either $\boldsymbol{\xi} = [\mathbf{0\ 0\ 0\ 0\ 0\ 0}]^{\boldsymbol{T}}$N or $\boldsymbol{\xi} = [\mathbf{20\ 0\ 0\ 0\ 0\ 0}]^{\boldsymbol{T}}$N. The results are given in Figures 19-20 which show good control of internal force and moment during the motion and excellent control of the position and orientation

of the object. To test the sensitivity of the controller to payload variation, the object weight was increased to 30N and the experiment repeated. The results are plotted in Figures 21-22. Internal force is controlled to within ±20% while position and orientation errors are kept well below 1mm and 1°, respectively.

VI. Conclusion

A simple robust internal force-based impedance control law for coordinating manipulators was presented which is computationally inexpensive and requires only minimal knowledge of each manipulator's inertia matrix. Since internal force is used in the impedance relationship, no knowledge of the object dynamics are required and object dynamics do not contribute to tracking and steady-state errors. The stability of the control system was analyzed including the effects of computational delays which showed that there exists a lower bound on the inertia matrix vis-a-vis the manipulator's estimated Cartesian end-point inertia which is independent of the sampling period and is valid under the rigid-body model assumption for the manipulators. Extensive experiments were conducted on a system consisting of two PUMA 560 manipulators which validate the proposed controller and showed that the system demonstrates excellent control of position and orientation along with the internal force and moment exerted on the object.

References

[1] S. Hayati, "Hybrid position/force control of multi-arm cooperating robots," in *Proceedings of the IEEE International Conference on Robotics and Automation*, pp. 82–89, 1986.

[2] M. Uchiyama and P. Dauchez, "A symmetric hybrid position/force control scheme for the coordination of two robots," in *Proceedings of the IEEE International Conference on Robotics and Automation*, pp. 350–356, 1988.

[3] E. Paljug, X. Yun, and V. Kumar, "Control of rolling contacts in multi-arm manipulation," *IEEE Transactions on Robotics and Automation*, vol. 10, pp. 441–452, Aug. 1994.

[4] S. Hayati, K. Tso, and T. Lee, "Generalized master/slave coordination and control for a dual-arm robotic system," in *Robots and Manufacturing*, (New York, NY), pp. 421–430, ASME Press, 1988.

[5] K. Kosuge, M. Koga, K. Furata, and K. Nosaki, "Coordinated motion control of robot arm based on virtual internal model," in *Proceedings of the IEEE International Conference on Robotics and Automation*, pp. 1097–1102, 1989.

[6] S. Schneider and R. Cannon, "Object impedance control for cooperative manipulation: Theory and experimental results," *IEEE Transactions on Robotics and Automation*, vol. 8, pp. 383–394, June 1992.

[7] J. Tao, J. Luh, and Y. Zheng, "Compliant coordination of two moving robots," *IEEE Transactions on Robotics and Automation*, vol. 6, pp. 322–330, June 1990.

[8] P. Chiacchio, S. Chiaverini, and B. Siciliano, "Cooperative control schemes for multiple robot manipulator systems," in *Proceedings of the IEEE International Conference on Robotics and Automation*, pp. 2218–2223, 1992.

[9] H. Kazerooni and T. Tsay, "Compliance control and unstructured modeling of cooperating robots," in *Proceedings of the IEEE International Conference on Robotics and Automation*, pp. 510–515, 1988.

[10] R. Bonitz and T. Hsia, "Internal force-based impedance control for cooperating manipulators," *IEEE Transactions on Robotics and Automation*, vol. 12, pp. 78–89, Feb. 1996.

[11] T. Hsia, "Simple robust schemes for cartesian space control of robot manipulators," *International Journal of Robotics and Automation*, vol. 9, no. 4, pp. 167–174, 1994.

[12] T. Hsia, T. Lasky, and Z. Guo, "Robust independent robot joint controller design for industrial robot manipulators," *IEEE Transactions on Industrial Electronics*, vol. 38, pp. 21–25, Feb. 1991.

[13] T. Hsia, "Decoupled robust joint control of robot manipulators," in *2nd International Workshop on Advanced Motion Control*, pp. 1–8, Mar. 1992. Nagoya, Japan.

[14] D. Whitney, "Historical perspective and state of the art in robot force control," in *Proceedings of the IEEE International Conference on Robotics and Automation*, pp. 262–268, 1985.

[15] J. Colgate, *The Control of Dynamically Interacting Systems.* PhD thesis, MIT, Aug. 1988.

[16] T. Hsia, "A new technique for robust conrol of servo systems," *IEEE Transactions on Industrial Electronics*, vol. 36, pp. 1–7, Feb. 1989.

[17] R. Bonitz and T. Hsia, "Force decomposition in cooperating manipulators using the theory of metric spaces and generalized inverses," in *Proceedings of the IEEE International Conference on Robotics and Automation*, vol. 2, pp. 1521–1527, May 1994.

[18] B. Armstrong, O. Khatib, and J. Burdick, "The explicit dynamic model and inertial parameters of the PUMA 560 arm," in *Proceedings of the IEEE International Conference on Robotics and Automation*, pp. 510–518, 1986.

[19] T. Kailath, *Linear Systems.* Prentice Hall, 1980.

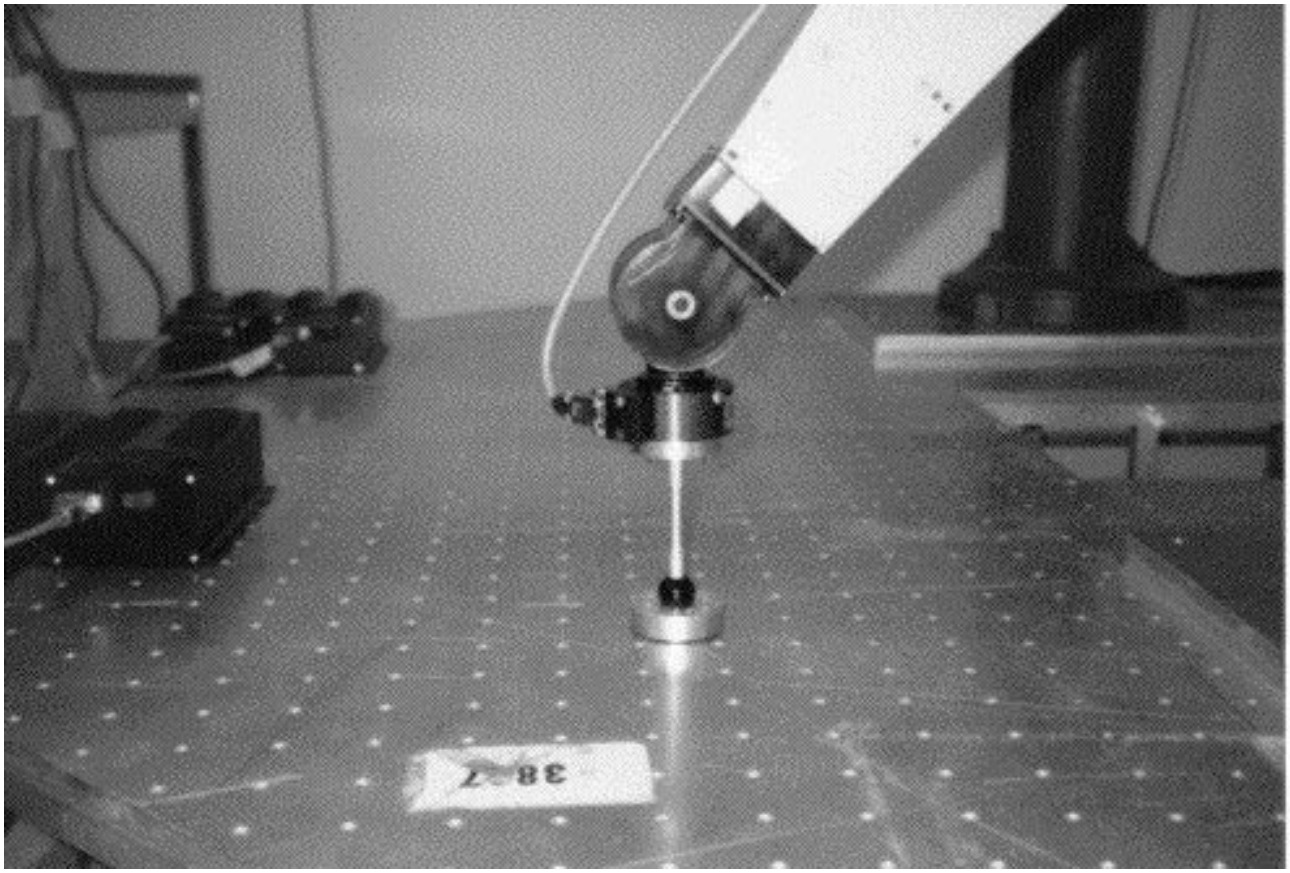

Fig. 5. Single-arm in Contact with Rigid Surface

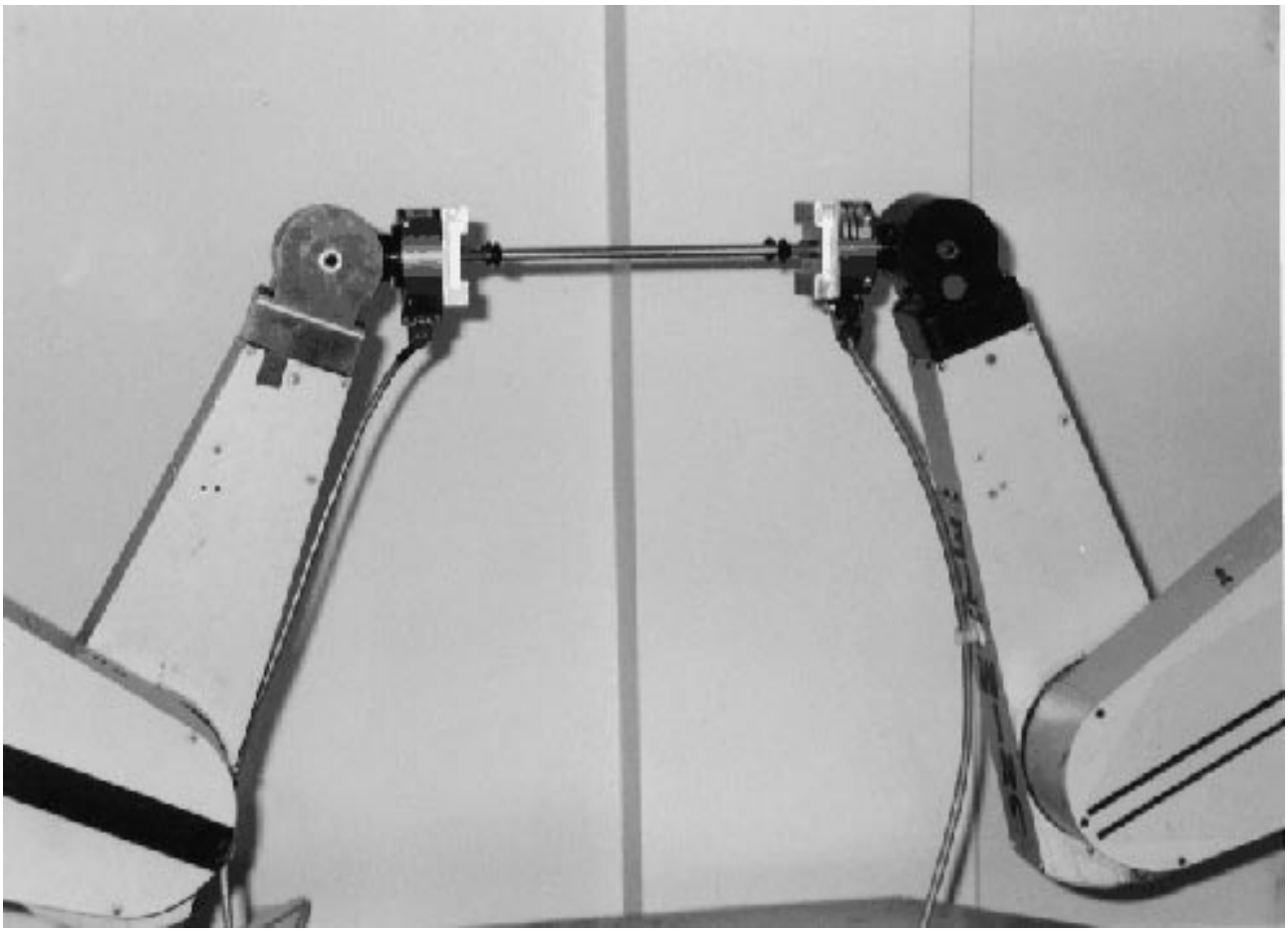

Fig. 6. Dual-arm Manipulation

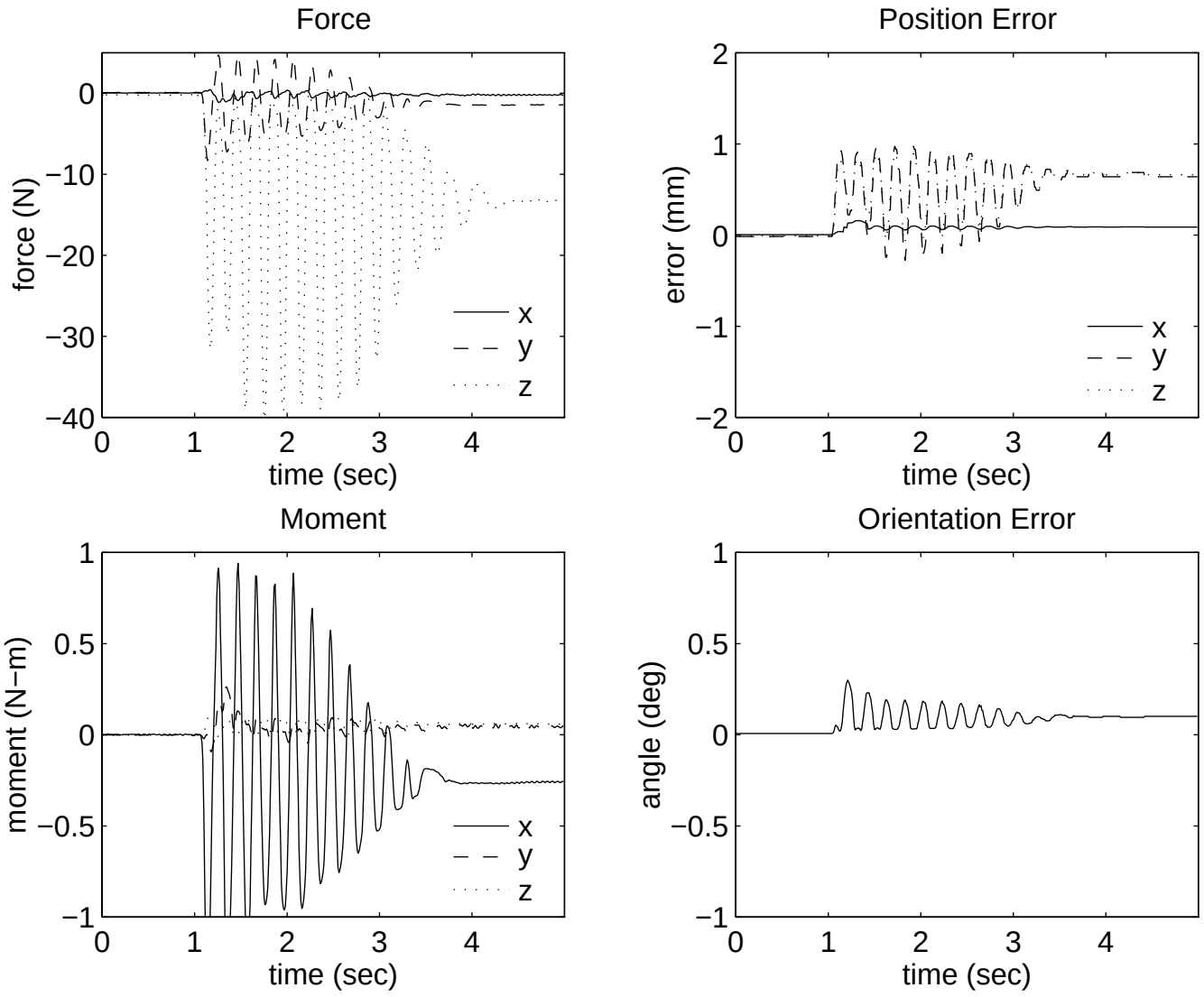

Fig. 7. Single-arm Step Response $\boldsymbol{M = 0.9 J^{-T} \bar{D} J^{-1}}$

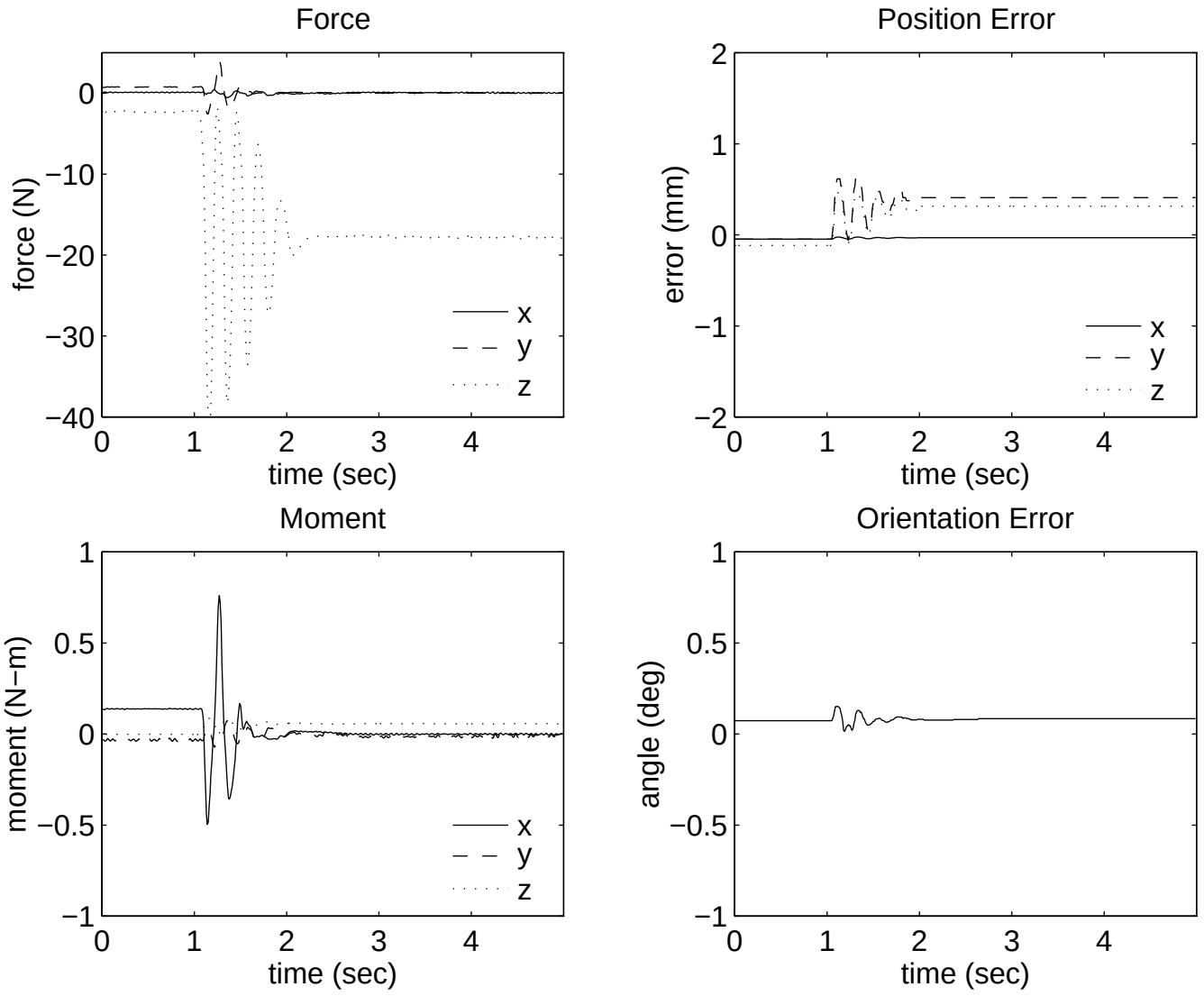

Fig. 8. Single-arm Step Response $\boldsymbol{M = J^{-T}\bar{D}J^{-1}}$

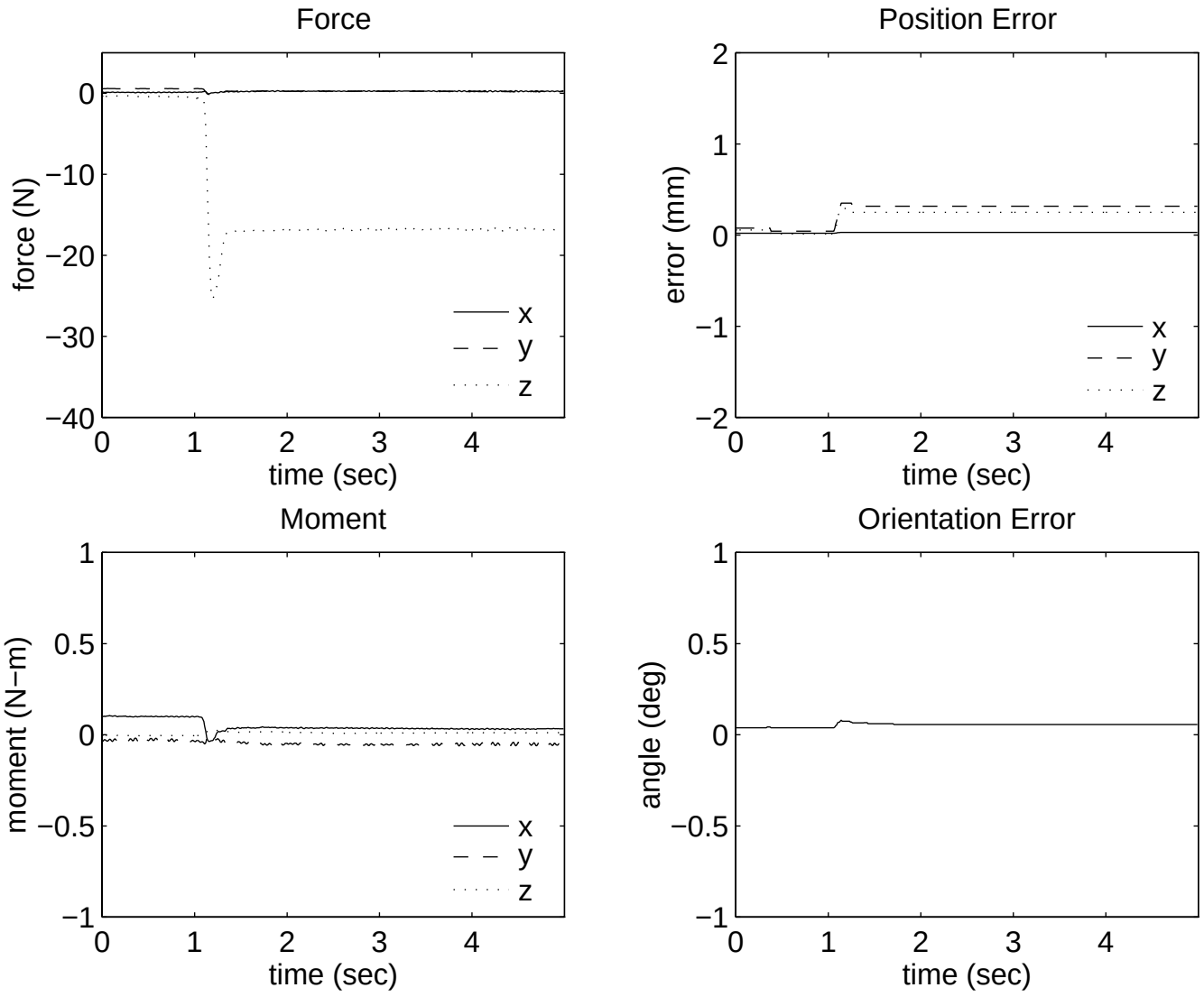

Fig. 9. Single-arm Step Response $\boldsymbol{M = 2J^{-T}\bar{D}J^{-1}}$

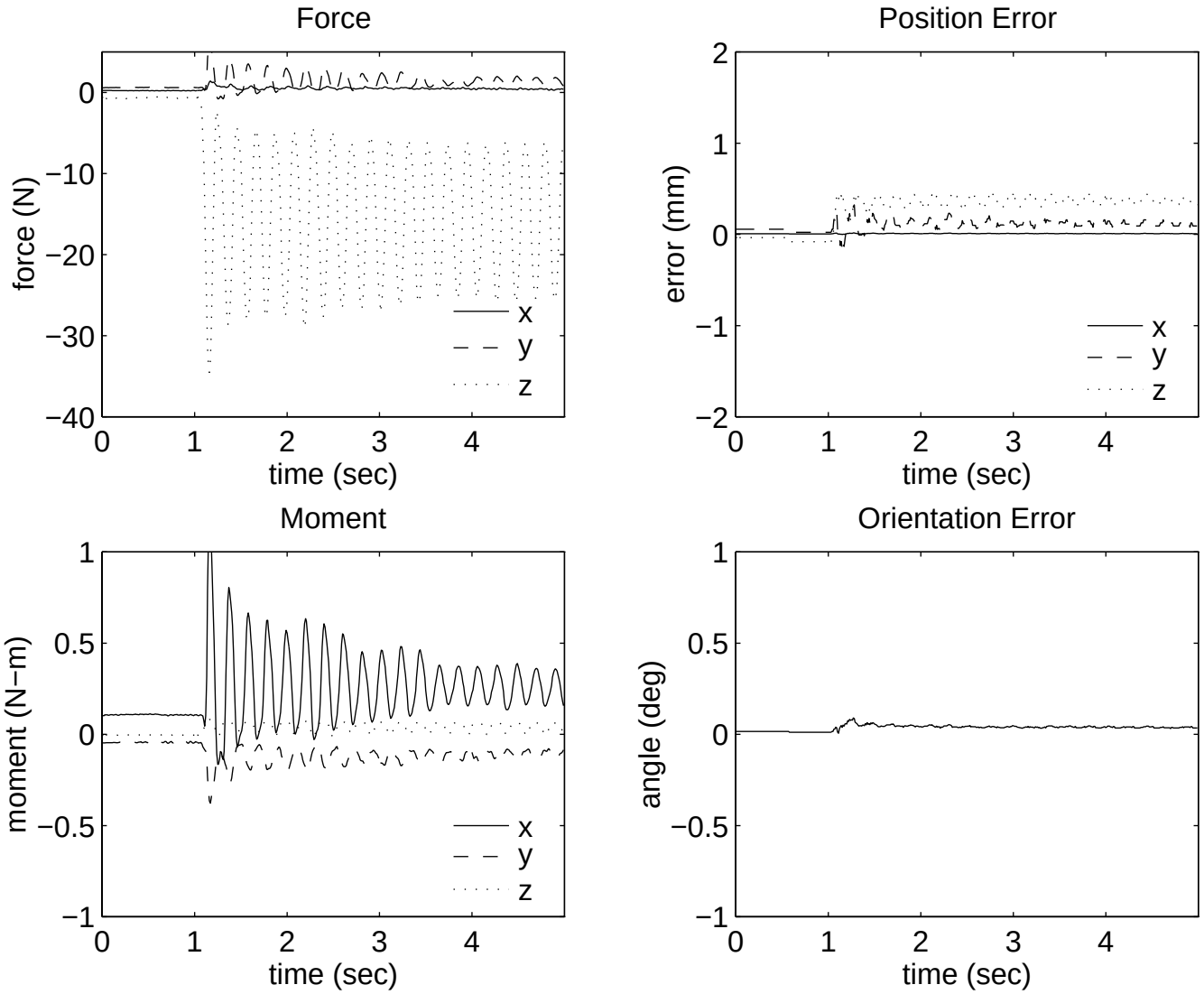

Fig. 10. Single-arm Step Response $(m_1, m_2) = (23, .8)$

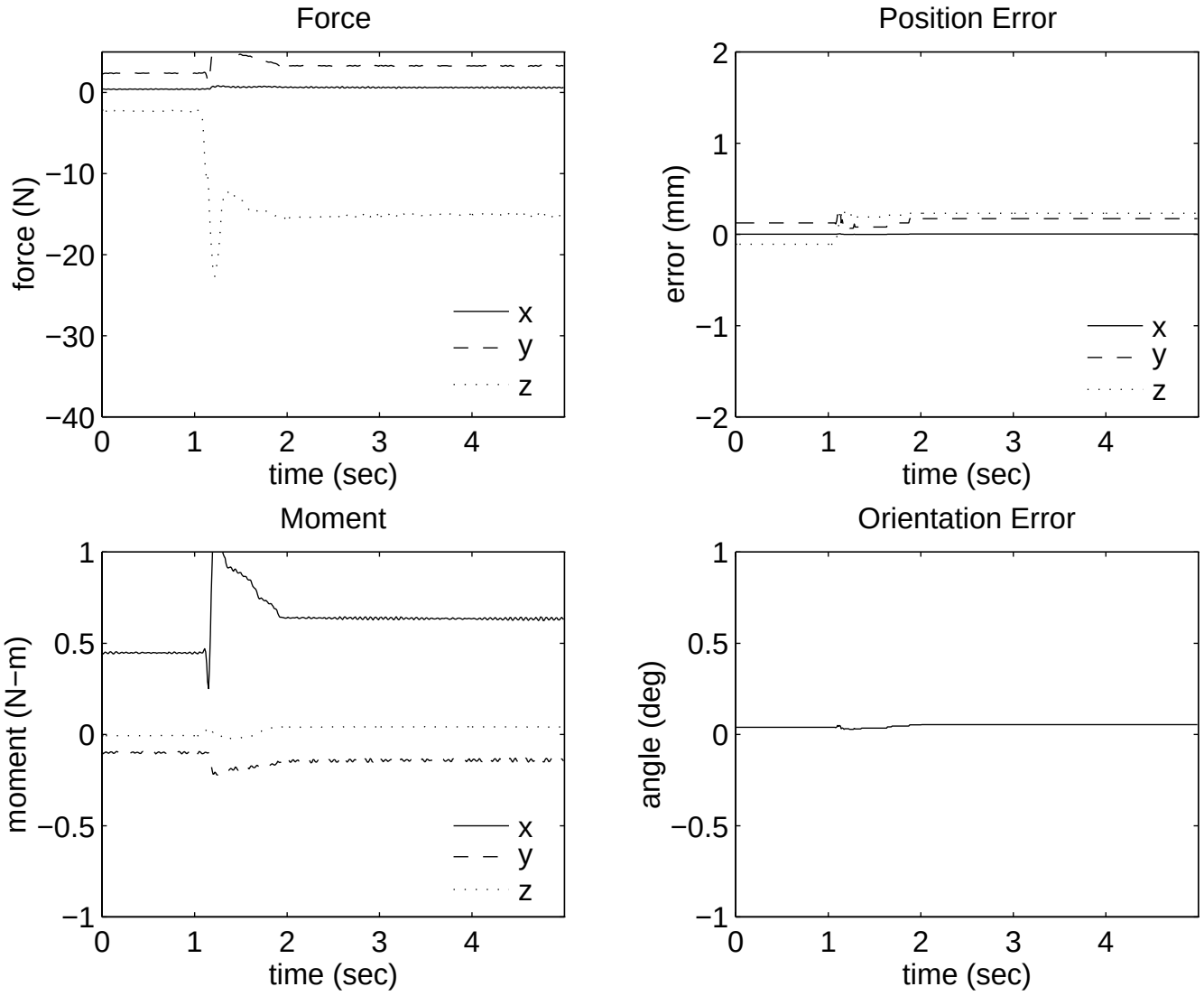

Fig. 11. Single-arm Step Response $(m_1, m_2) = (36, 1.3)$

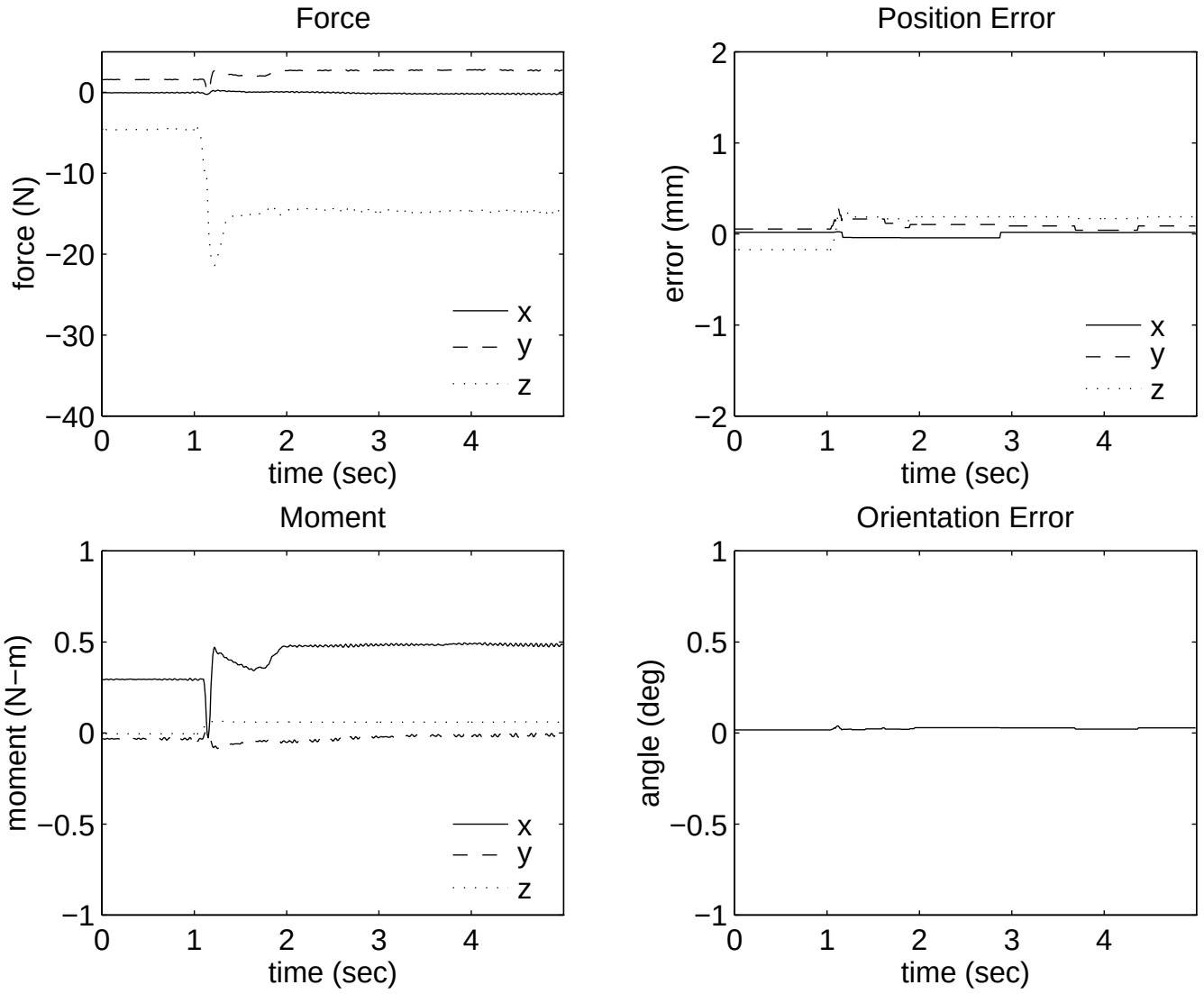

Fig. 12. Single-arm Step Response $(m_1, m_2) = (50, 1.8)$

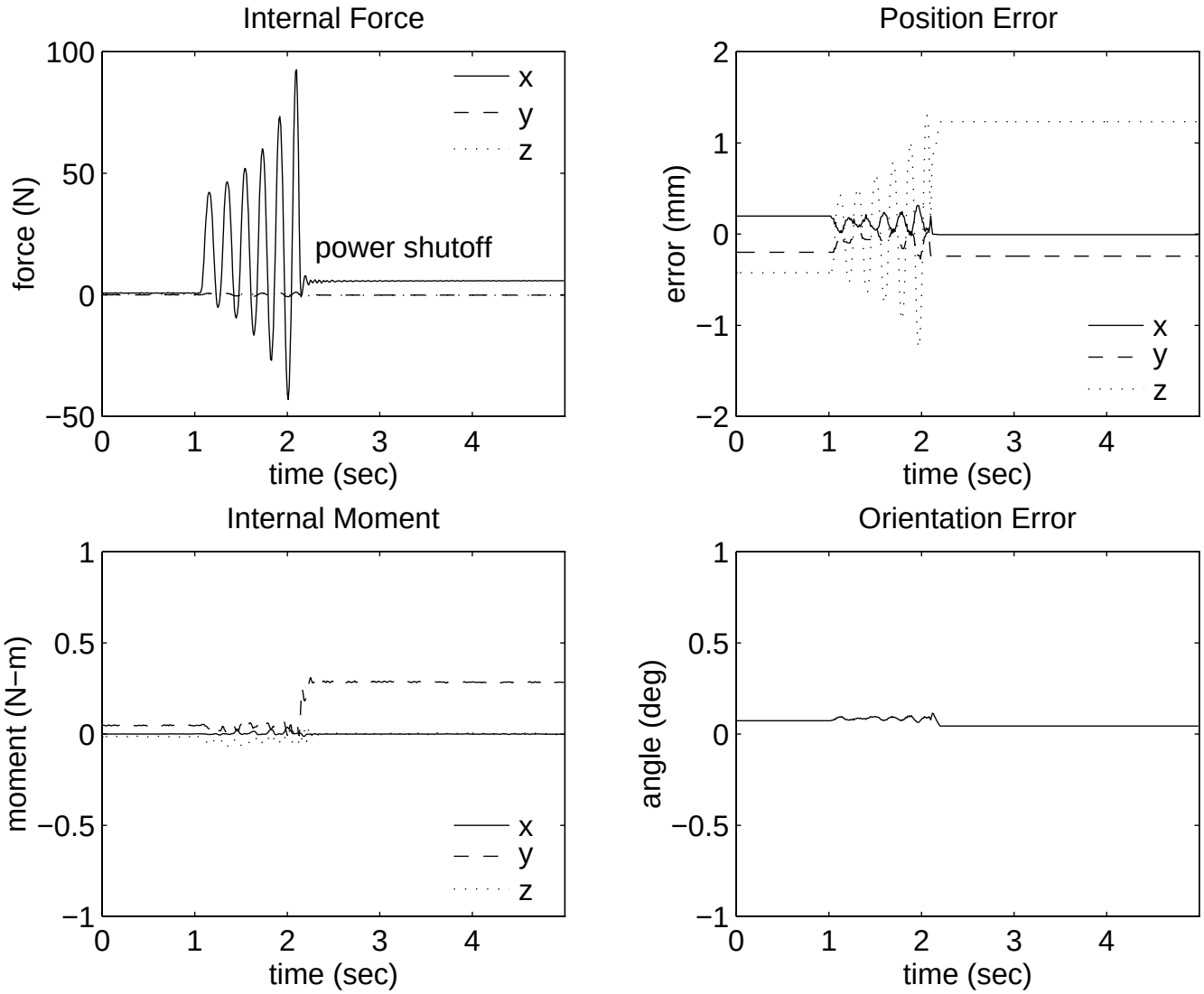

Fig. 13. Dual-arm Step Response $\boldsymbol{M_i = 0.9 J_i^{-T} \bar{D}_i J_i^{-1}}$

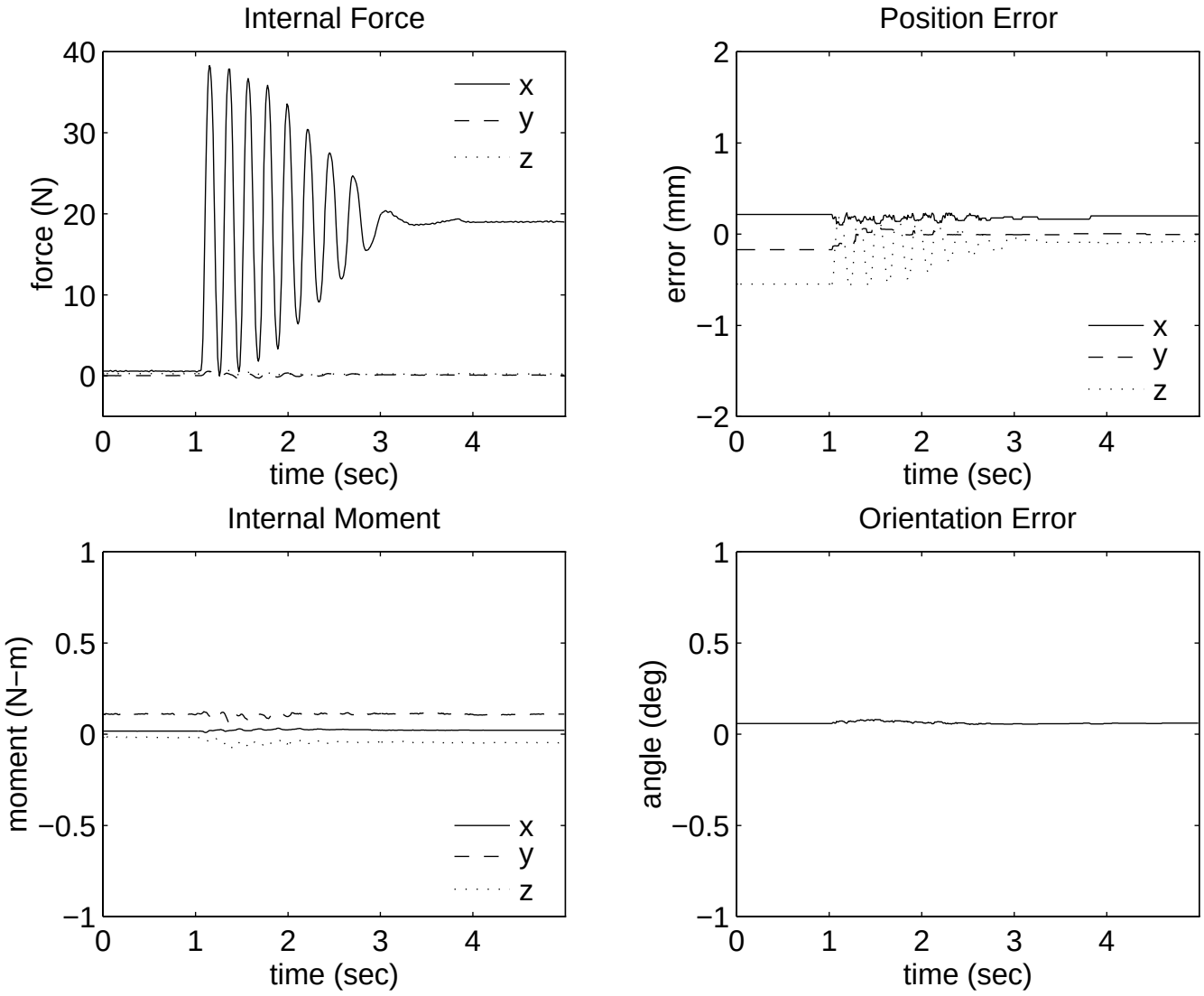

Fig. 14. Dual-arm Step Response $\boldsymbol{M_i = J_i^{-T} \bar{D}_i J_i^{-1}}$

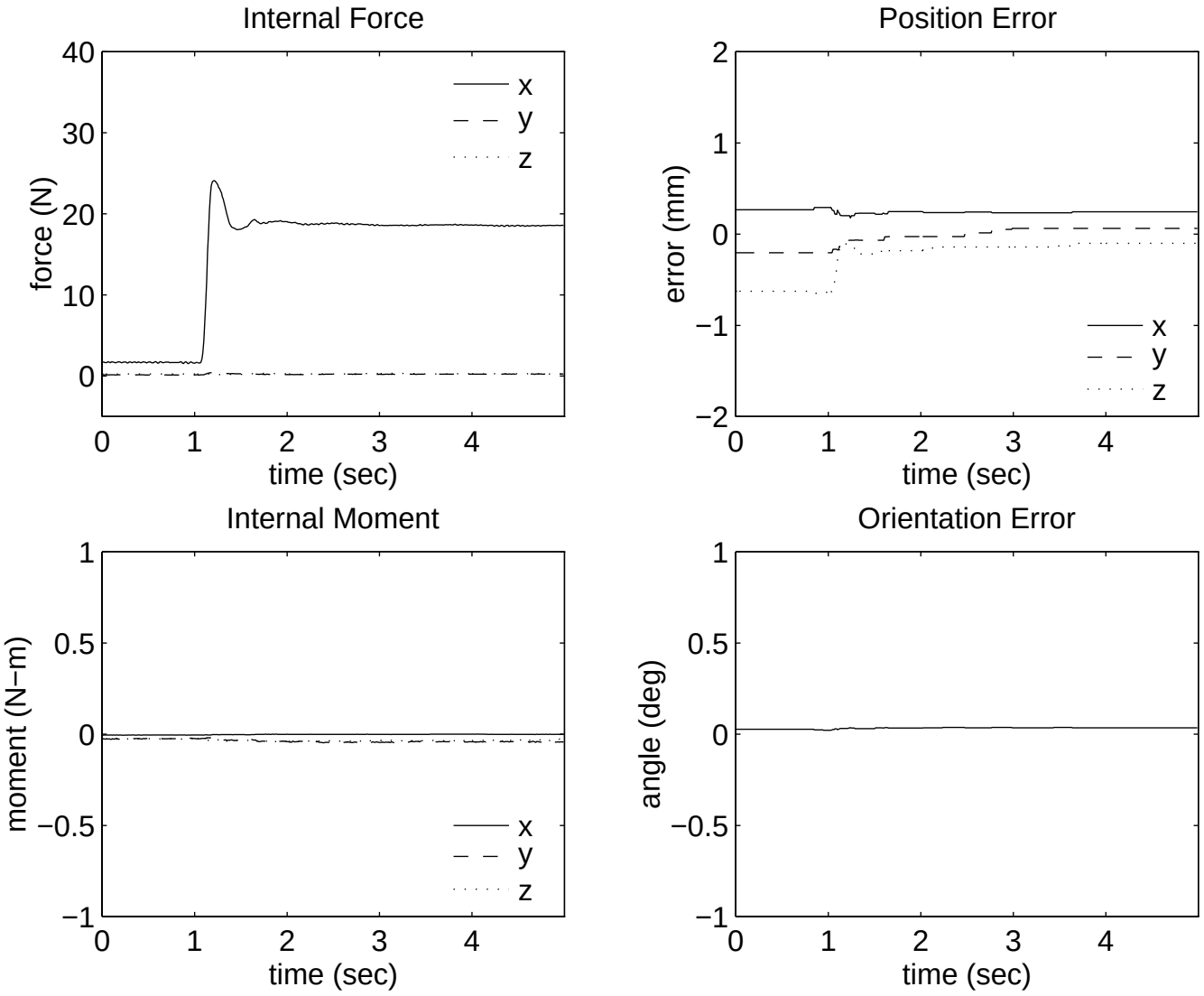

Fig. 15. Dual-arm Step Response $\boldsymbol{M_i = 2J_i^{-T}\bar{D}_i J_i^{-1}}$

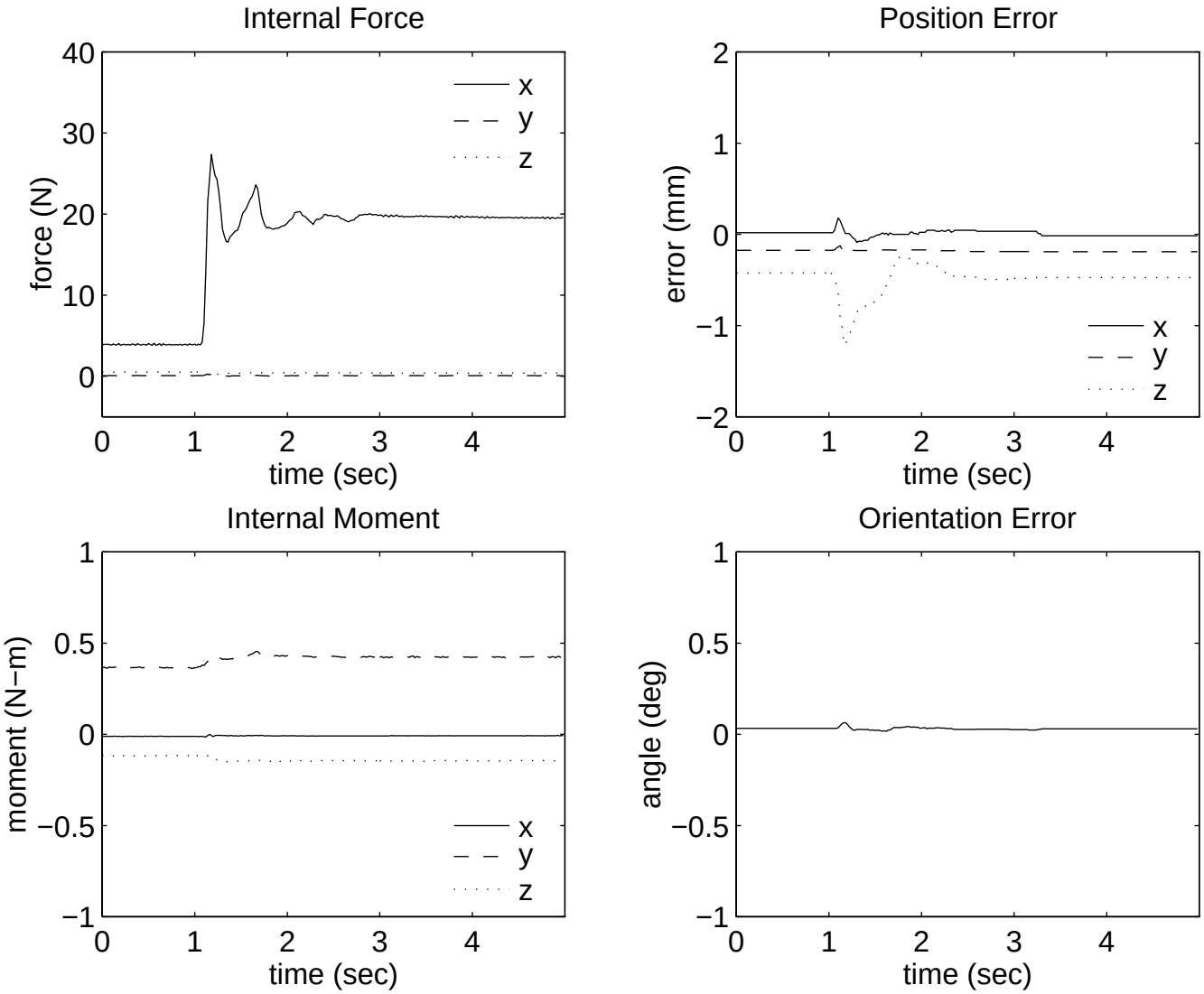

Fig. 16. Dual-arm Step Response $(m_1, m_2) = (11, .4)$

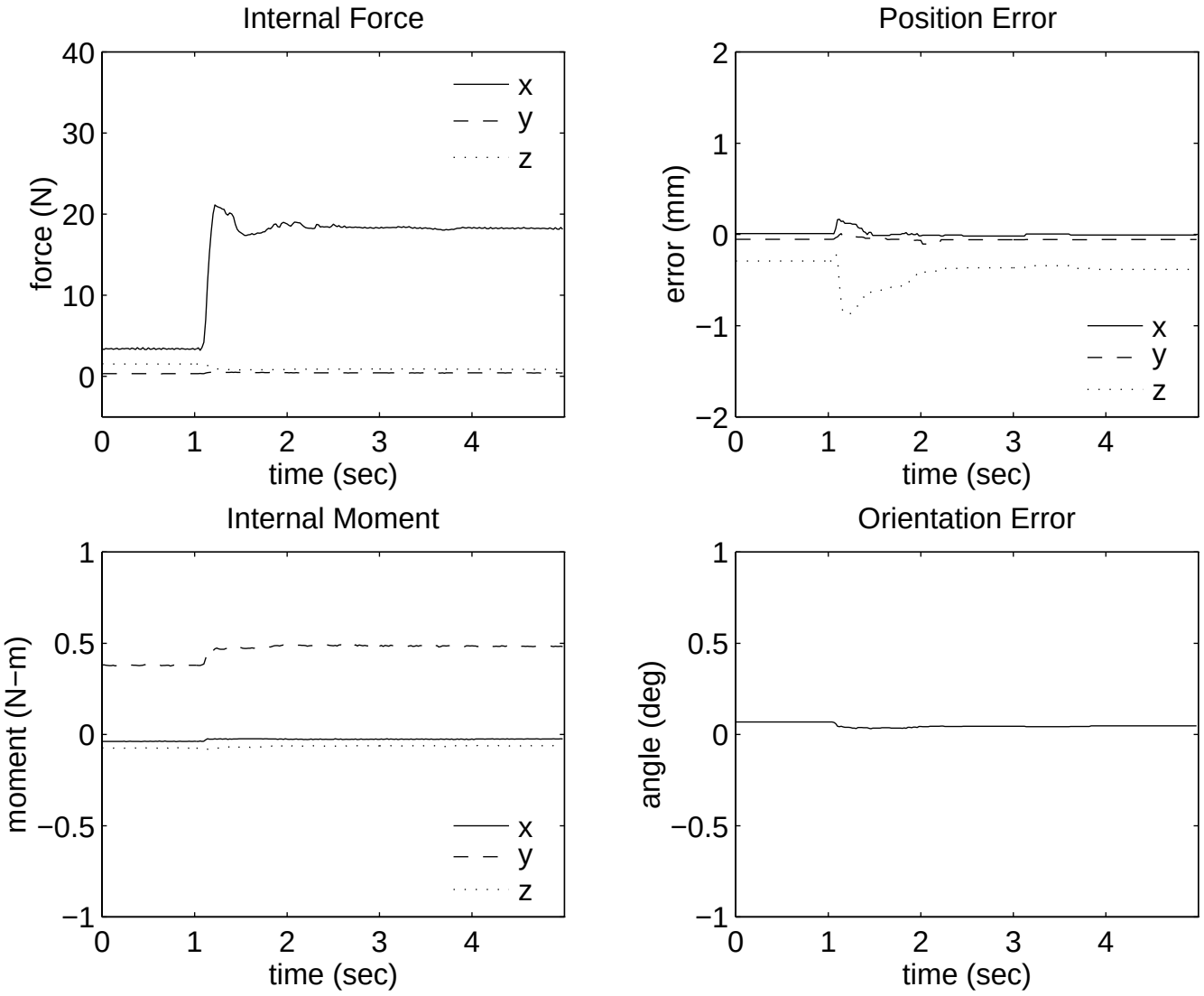

Fig. 17. Dual-arm Step Response $(m_1, m_2) = (18, .6)$

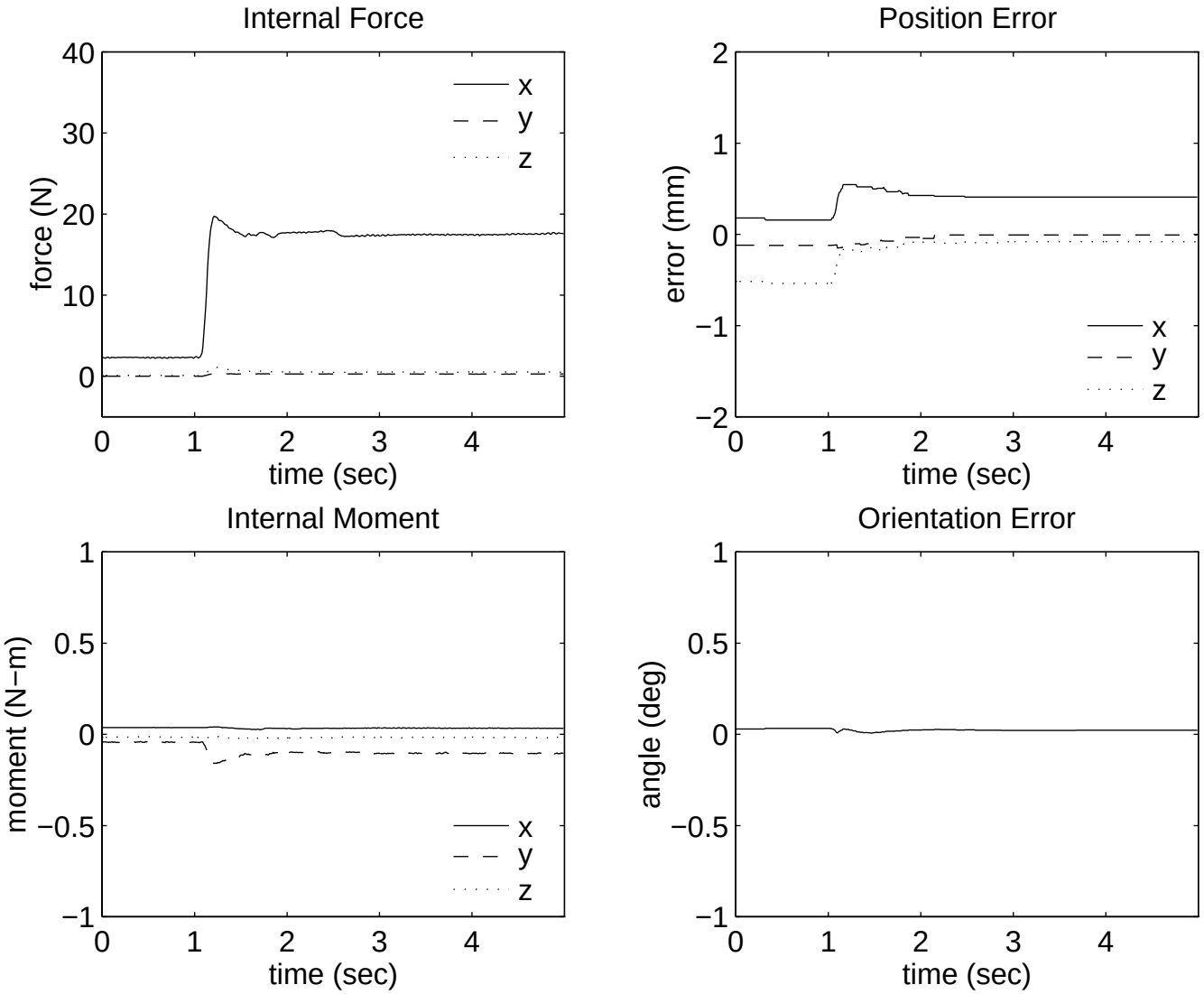

Fig. 18. Dual-arm Step Response $(m_1, m_2) = (37, 1.3)$

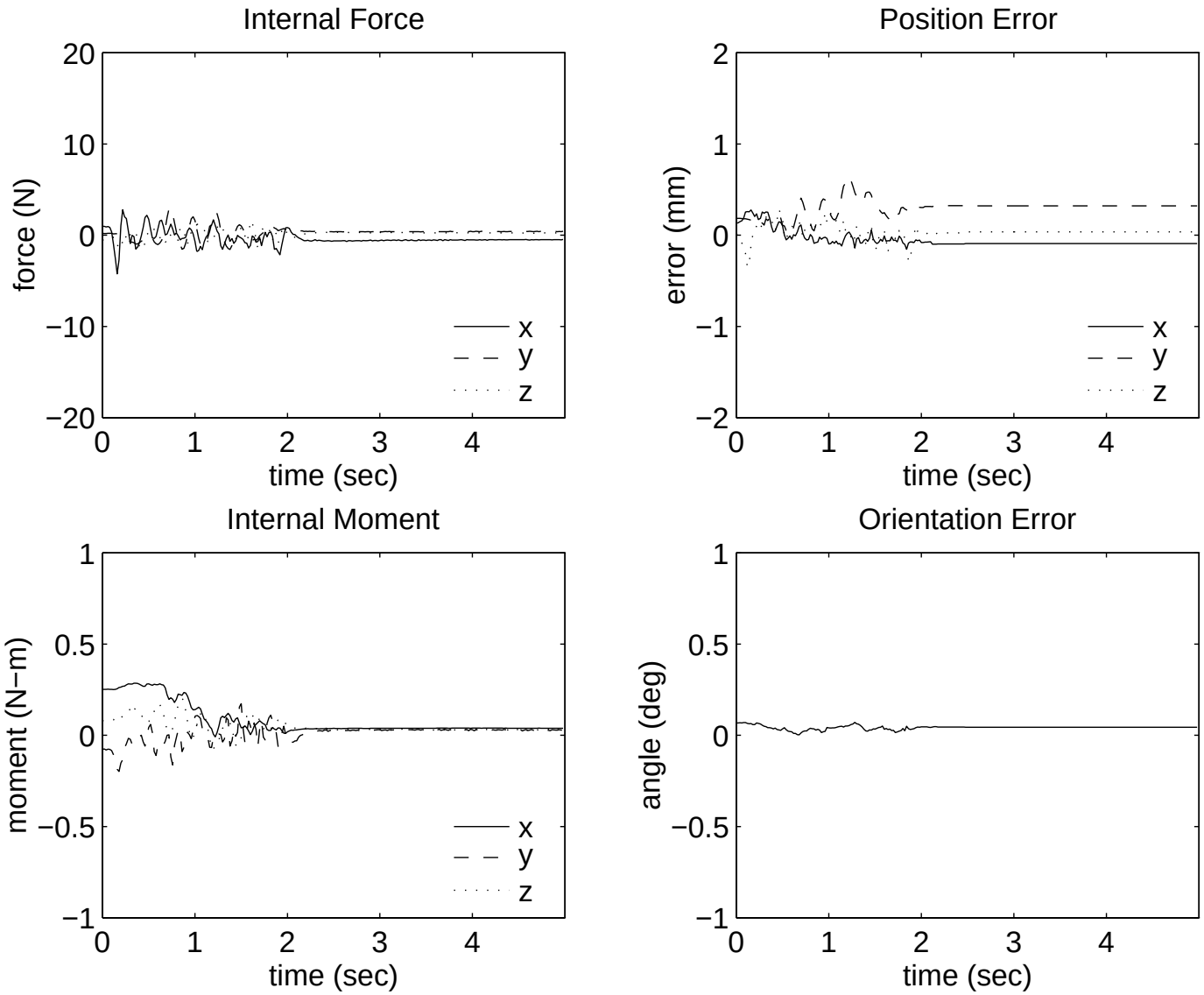

Fig. 19. Dual-arm Motion - Object=8N, ξ=0N

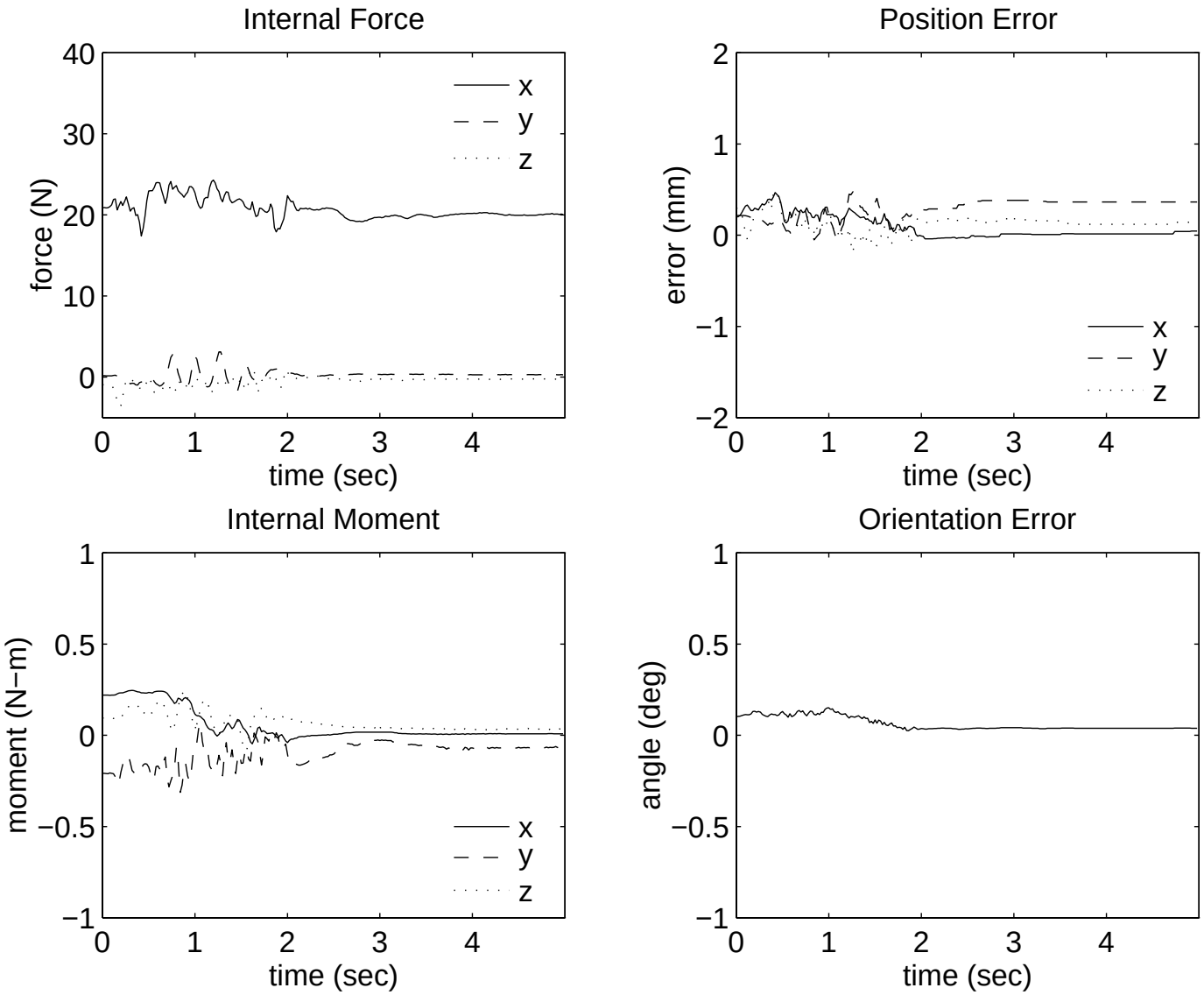

Fig. 20. Dual-arm Motion - Object=8N, ξ=20N

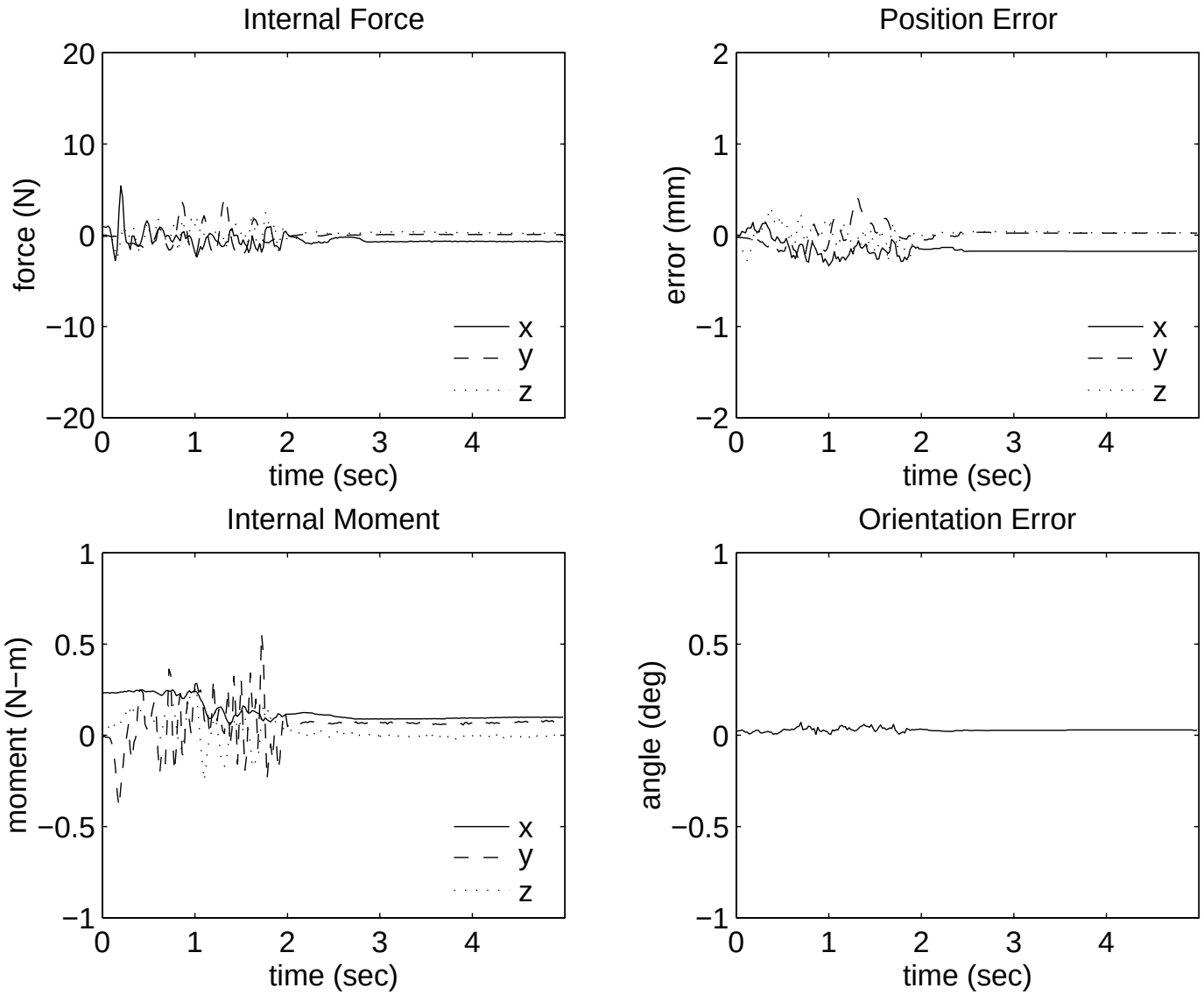

Fig. 21. Dual-arm Motion - Object=30N, $\boldsymbol{\xi}$=0N

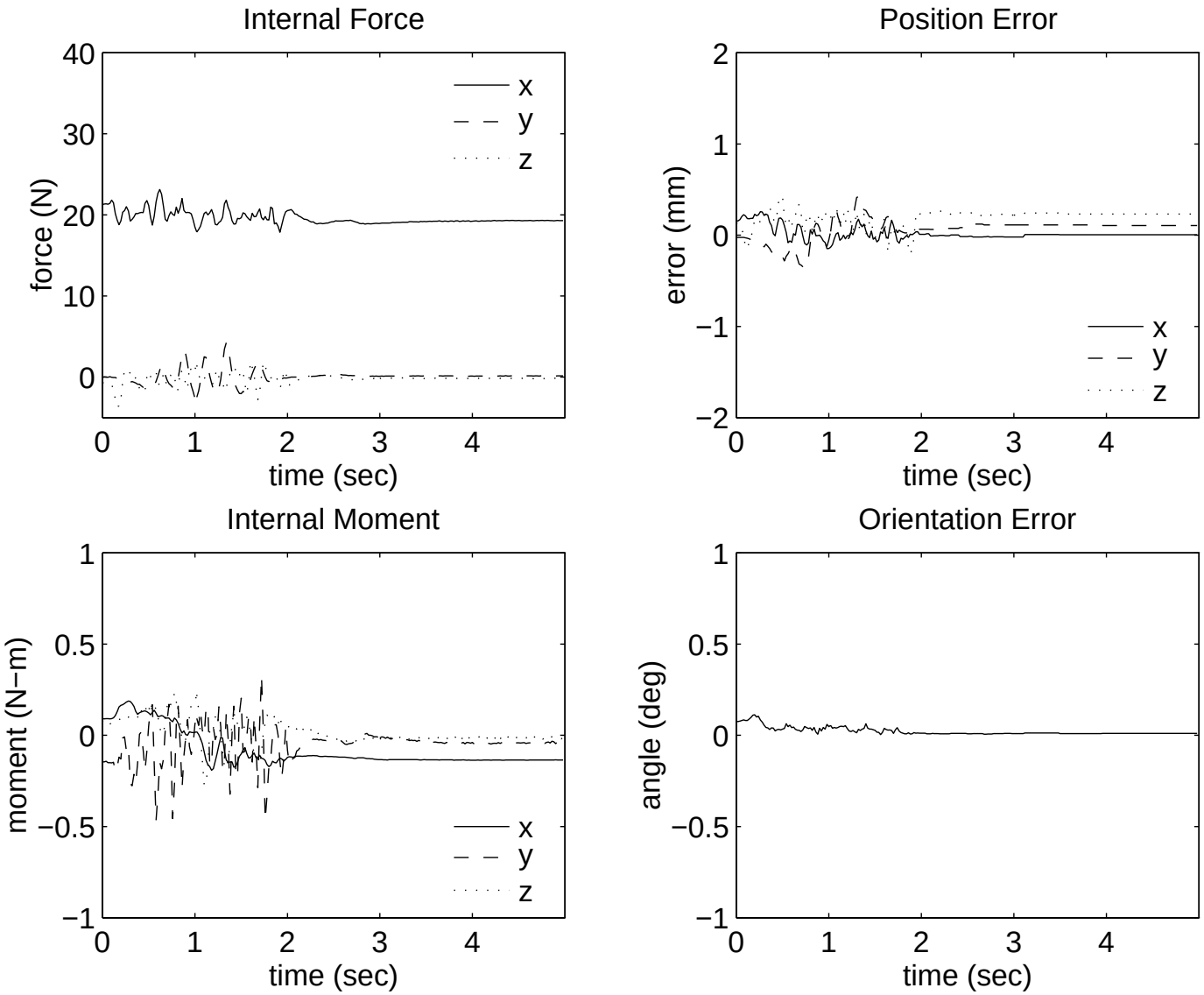

Fig. 22. Dual-arm Motion - Object=30N, ξ=20N